

Heterogeneous Electrocatalysis of Carbon Dioxide to Methane

Yugang Wu , Huitong Du, Peiwen Li, Xiangyang Zhang, Yanbo Yin and Wenlei Zhu * 

State Key Laboratory of Pollution Control and Resource Reuse, State Key Laboratory of Analytical Chemistry for Life Science, the Frontiers Science Center for Critical Earth Material Cycling, School of the Environment, School of Chemistry and Chemical Engineering, Nanjing University, Nanjing 210023, China

* Correspondence: wenleizhu@nju.edu.cn

Abstract: Electrocatalytic CO₂ reduction to valued products is a promising way to mitigate the greenhouse effect, as this reaction makes use of the excess CO₂ in the atmosphere and at the same time forms valued fuels to partially fulfill the energy demand for human beings. Among these valued products, methane is considered a high-value product with a high energy density. This review systematically summarizes the recently studied reaction mechanisms for CO₂ electroreduction to CH₄. It guides us in designing effective electrocatalysts with an improved electrocatalytic performance. In addition, we briefly summarize the recent progress on CO₂ electroreduction into CH₄ from the instructive catalyst design, including catalyst structure engineering and catalyst component engineering, and then briefly discuss the electrolyte effect. Furthermore, we also provide a simplified techno-economic analysis of this technology. These summaries are helpful for beginners to rapidly master the contents related to the electroreduction of carbon dioxide to methane and also help to promote the further development of this field.

Keywords: carbon dioxide reduction; methane; electrocatalysts; techno-economic analysis



Citation: Wu, Y.; Du, H.; Li, P.; Zhang, X.; Yin, Y.; Zhu, W. Heterogeneous Electrocatalysis of Carbon Dioxide to Methane. *Methane* **2023**, *2*, 148–175. <https://doi.org/10.3390/methane2020012>

Academic Editor: Mateusz Wnukowski

Received: 29 November 2022

Revised: 10 April 2023

Accepted: 14 April 2023

Published: 17 April 2023



Copyright: © 2023 by the authors. Licensee MDPI, Basel, Switzerland. This article is an open access article distributed under the terms and conditions of the Creative Commons Attribution (CC BY) license (<https://creativecommons.org/licenses/by/4.0/>).

1. Introduction

Anthropogenic activities, particularly the extensive utilization of fossil fuels, have caused a significant increase in atmospheric CO₂ concentrations, exacerbating the ongoing climate change crisis. Increased levels of CO₂ lead to a heightened greenhouse effect, resulting in several adverse impacts on the global climate, including an increase in temperatures and sea level, altered precipitation patterns, and an increased frequency and intensity of natural disasters. These phenomena, in turn, have far-reaching ecological, social, and economic consequences, such as habitat destruction, species extinction, displacement of populations, and loss of biodiversity. Therefore, it is imperative to adopt sustainable energy sources and practices that reduce our dependence on fossil fuels to mitigate the detrimental effects of climate change and ensure a sustainable future for the planet and its inhabitants [1–7]. Thus, the reduction of CO₂ to carbon-containing fuels is a promising technology for reducing CO₂ emissions and achieving a sustainable future. This approach allows the conversion of intermittent renewable energy into high-energy fuels, providing a pathway to reduce our reliance on fossil fuels. Additionally, integrating CO₂ into the global energy cycle through hydrocarbon synthesis allows us to achieve true global carbon neutrality [8–13]. At present, the main technologies aimed at reducing CO₂ emissions include photo-, electro-, bio-, thermal, and their synergistic catalyses [14–19]. Each of these methods has its own set of advantages and limitations. For instance, photocatalysis is easy to perform and has a broad range of applications; however, it suffers from poor catalyst stability and lifespan [20]. Biocatalysis involves using biological enzymes to catalyze CO₂ in mild-reaction conditions with good selectivity; however, yields are often low and catalyst deactivation is a common issue [21]. In this context, we focus on electrocatalytic technology due to its rapid reaction rate, excellent selectivity, and established industrial infrastructure. Additionally, the proportion of electricity generated by renewable energy sources is

increasingly significant in the total electricity mix [22]. Additionally, the process offers a means of energy storage, making it a viable option for balancing the fluctuating supply and demand of energy. However, the development of cost-effective, large-scale CO₂RR systems is crucial for the successful deployment of this technology. Further research and technological advancements in this area are necessary to advance toward a carbon-neutral future [5,23–29].

Methane, which is among the products of CO₂RR, is regarded as a high-value commodity due to its high energy density of 55.5 MJ/kg. Moreover, the methane produced by the electrochemical reduction of CO₂ is not emitted into the atmosphere and contributes to the greenhouse effect as the well-established infrastructure for gas pipelines, allowing for the seamless storage, consumption, and distribution of methane, rendering it a widely utilized component of natural gas. With a composition of 21.4% of total primary energy, methane boasts a high abundance and is an attractive candidate for various energy applications [30–34]. Concomitantly, contemporary technology offers the potential to convert CH₄ into fundamental chemicals through various routes, such as the oxidative conversion into syngas or direct conversion into other chemical compounds [35–38]. Even after the inevitable transition to thermonuclear energy in the distant future, methane remains the most portable, easily stored, and transported fuel and general-purpose chemical raw material [39]. Most importantly, the next generation of rocket fuel will be liquid methane; the in situ production of methane as rocket fuel on alien planets, such as Mars, will become a key technology for human interstellar navigation. Therefore, the development of CO₂RR technology to prepare high amounts of CH₄ is necessary for this application.

However, it is unfavorable to convert CO₂ into CH₄ due to the presence of π bonds in CO₂ molecules. In addition to the limitation of sluggish reaction kinetics, the hydrogen evolution reaction (HER) will also compete with CO₂RR [40]. To solve the abovementioned challenges, developing electrode catalysts with a high efficiency and good selectivity is necessary and urgent. In recent years, numerous efforts have been devoted to the design and synthesis of suitable heterogeneous electrocatalysts for the electrocatalytic reduction of CO₂, and some of them have shown outstanding CH₄ selectivity [41]. To a certain extent, some of the problems have been solved; however, there are still challenges to be faced concerning the CO₂RR to CH₄ formation process. Therefore, understanding the reaction mechanism and a summary of the related work based on the CO₂RR to CH₄ formation process are necessary, which will contribute to further developments in the field.

Although methane has the advantages of its high calorific value and well-established transportation infrastructure, the market price of methane is relatively low because the development of the technology to exploit shale gas and methane hydrate result in a large global methane supply. Hence, it is imperative to perform a technical–economic analysis of the industrial implementation of CO₂ electrolysis concerning CH₄ formation. Techno-economic analysis is a fundamental tool for assessing the economic benefits and costs of emerging technologies in practical applications. An assessment of the technical and economic aspects of a novel technology is an indispensable step in the process of translating it from the research into practical application [42–45]. In the context of the electrocatalytic reduction of CO₂ for the formation of CH₄, a comprehensive economic analysis can provide valuable guidance to researchers for developing catalysts that are more responsive to the complex and dynamic demands of the market.

In this review, we summarize the latest progress in CO₂RR for the selective electrocatalytic reduction of CO₂ to CH₄ in an aqueous solution based on heterogeneous catalysts. Firstly, we discuss the reaction mechanisms and electrolyte effect, fundamentally, which provides an insight into designing electrolyzers and electrocatalysts with an improved performance. Then, we focus on several electrocatalysts with an excellent catalytic performance and great development potential. A prevalent characteristic shared among the majority of these electrocatalysts is the presence of the copper element, which is expounded upon in the section on the reaction mechanism. In addition, we provide a simplified techno-economic analysis for this technology. Finally, we anticipate electrochemical catalysts'

further development prospects and challenges. We are confident that this review will be helpful for beginners in this field and will further advance the development of CO₂RR.

2. Reaction Mechanism

Many research efforts have attempted to discover the mechanism of the electrochemical reduction of CO₂ to CH₄ from both experimental [46–49] and computational points of view [49–54]. From the pure-thermodynamics point of view, it is possible to reduce carbon dioxide to CH₄ at a potential of + 0.17 V vs. reversible hydrogen electrode (RHE) [55] (Table 1). However, numerous studies have shown that CO₂ electrochemical reduction to CH₄ consists of multiple elementary steps [47,52]. As shown in Figure 1A, CO₂ is firstly absorbed on the catalyst and hydrogenated into *COOH via an electron transfer–proton coupling process [51]. Then, the *COOH is further evolved into *CO, which is the main branch point to determine whether or not to produce oxygen-containing products. In path I, *CO goes through a CHO* intermediate, with the overall path proceeding as:



(the H⁺ + e[−] reactants and H₂O product formed were left off).

The step to determine the selectivity is the final CH₃O* reduction step. It was found that the production of CH₄ had a more favorable reaction-free energy. In path II, *CO goes through a COH* intermediate with the overall path proceeding as:



(the H⁺ + e[−] reactants and H₂O products formed were left off).

Notably, from Peterson et al.'s work, we know that the absorption energy of the intermediate is crucial for product distributions [56]. For example, the metals (Au, Ag, and Zn) with weak *CO-bound energy produce little methane because CO experiences priority desorption before any further reductions occur [57–59]. Additionally, metals (Pt, Pd, and Ni) with strong *CO-bound energy cannot remove the *CO from the surface because of the highly unfavorable thermodynamic conditions. Thus, CO₂ can only be reduced further to CH₄ with an exceedingly low Faraday efficiency (FE) on these electrodes [60]. In contrast, the metal Cu is located near the top of the volcano curve of the limit potential. This means that the *CO-adsorption intensity of Cu is suitable for CH₄ production via the CO₂RR process (Figure 1B–D).

Table 1. Half reactions and potentials of CO₂ electrochemical-reduction reactions.

Half-Reactions Formula	Electrode Potential/V (vs. RHE)
$\text{CO}_2 + \text{H}_2\text{O} + 2\text{e}^- \rightarrow \text{CO} + 2\text{OH}^-$	−0.10
$\text{CO}_2 + 2\text{H}_2\text{O} + 2\text{e}^- \rightarrow \text{HCOOH} + 2\text{OH}^-$	−0.20 (pH < 4); −0.20 + 0.059 (pH > 4)
$\text{CO}_2 + 3\text{H}_2\text{O} + 4\text{e}^- \rightarrow \text{HCHO} + 4\text{OH}^-$	−0.07
$\text{CO}_2 + 5\text{H}_2\text{O} + 6\text{e}^- \rightarrow \text{CH}_3\text{OH} + 6\text{OH}^-$	0.02
$\text{CO}_2 + 6\text{H}_2\text{O} + 8\text{e}^- \rightarrow \text{CH}_4 + 8\text{OH}^-$	0.17
$2\text{CO}_2 + 8\text{H}_2\text{O} + 12\text{e}^- \rightarrow \text{C}_2\text{H}_4 + 12\text{OH}^-$	0.08
$2\text{CO}_2 + 9\text{H}_2\text{O} + 12\text{e}^- \rightarrow \text{CH}_3\text{CH}_2\text{OH} + 12\text{OH}^-$	0.09

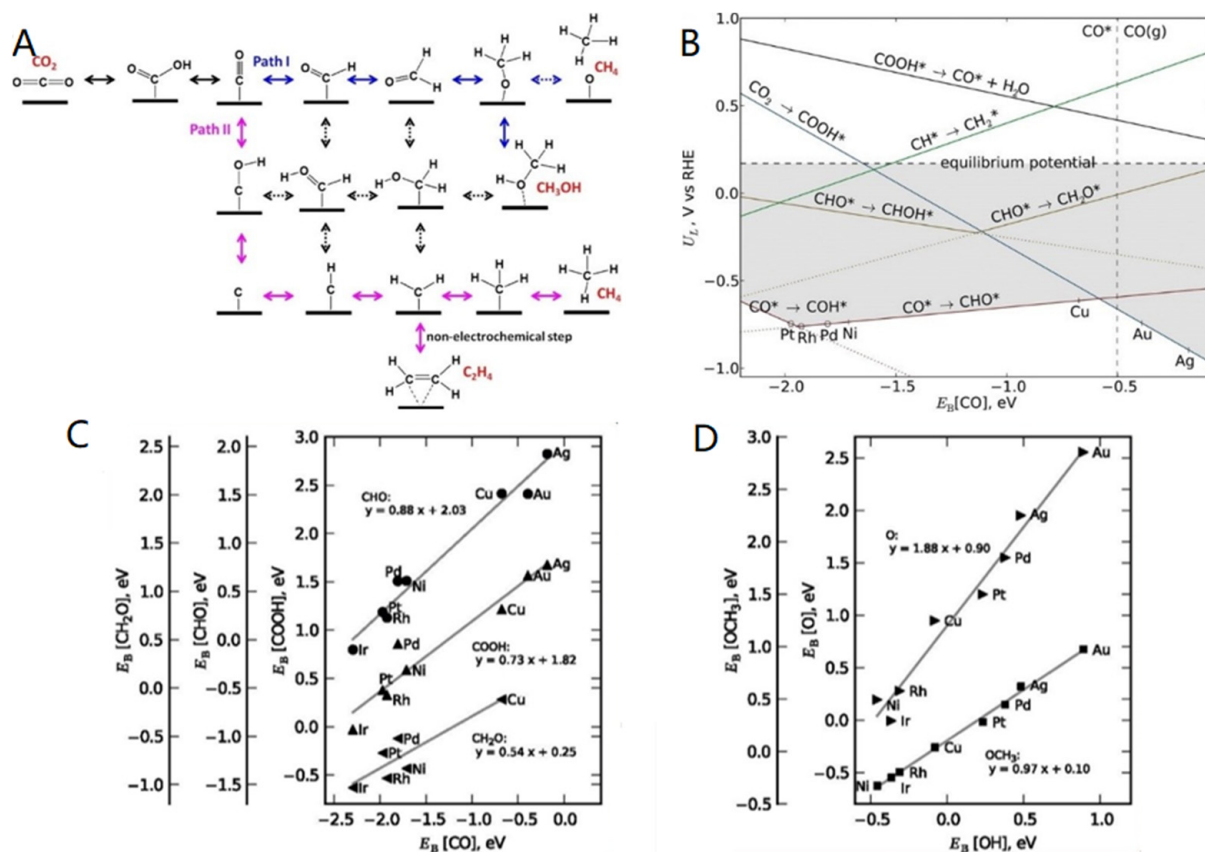


Figure 1. (A) Pathway of CO₂RR for CH₄ formation on Cu (111). Reproduced with permission from Ref. [13]; (B) volcano plot of limiting potentials versus CO-binding strength for CO₂ reduction; (C,D) linear energetic scaling relationships between absorption energy of CO (EB) and certain adsorbed intermediates. Reproduced with permission from Ref. [56].

Notably, some details of the reactions may be slightly different from what was mentioned above over different CO₂RR catalysts. As shown in Figure 2A, Dong et al. [61] reported that *CO protonated through a similar bridge configuration on the Cu₂O/Cu interface. This conclusion was confirmed by the density functional theory (DFT) calculation. Interestingly, they also found that the Cu₂O/Cu interface formed during the electrochemical reaction process played a crucial role in determining the selectivity of methane formation, which may indicate that the crystal plane is not the key factor for the CO₂RR to CH₄ formation process on reconstructed Cu₂O microparticles.

As for the surface-reaction mechanism, two hypotheses were proposed, which are the Eley–Rideal (H comes from the solution) and Langmuir–Hinshelwood (H comes from the surface-adsorbed hydrogen (*H)) mechanisms, respectively (Figure 2B,C). Yogesh and coworkers [62] studied the mechanism of electrochemical CO₂ reduced to CH₄ on the surface of Cu. They found that the methane production rate was significantly suppressed when increasing the pressure of CO. However, for the Eley–Rideal mechanism, the reaction rate should be positively correlated with the pressure of CO, which was inconsistent with the experimental phenomena. The experimental result thus excludes the Eley–Rideal mechanism and strongly supports the Langmuir–Hinshelwood mechanism, where CO_{ads} and H_{ads} are in competition with each other for surface sites. The result was also confirmed by Asthagiri and coworkers' works with the DFT calculation [51].

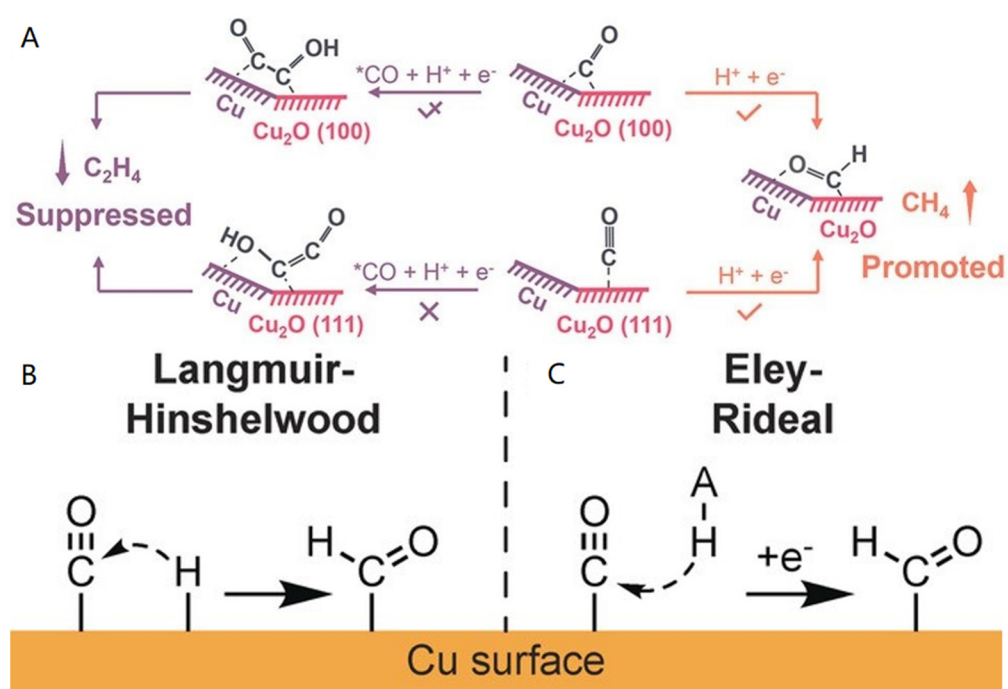


Figure 2. (A) Reaction pathway and adsorption site of *CO protonation to *CHO , as well as C–C coupling to *OCCOH on reconstructed $c\text{-Cu}_2\text{O}/\text{Cu}$ and $o\text{-Cu}_2\text{O}/\text{Cu}$ interfaces. Reproduced with permission from Ref. [61]; (B) Langmuir–Hinshelwood mechanism; (C) Eley–Rideal mechanism. Reproduced with permission from Ref. [62].

3. Electrolyte Effect

3.1. CO_2 Reduction in Aqueous Electrolytes

A mild-reaction condition is usually associated with decreased expenses. Additionally, a lab reactor, such as H-shaped electrochemical and flow cells, is present in an aqueous environment with alkaline electrolytes [63–65]. Thus, understanding the reaction condition in an aqueous environment and the corresponding influencing factors is very helpful.

The environment near the interface of the catalysts, such as the pH and concentration of CO_2 , is different from bulk electrolytes [66,67]. Therefore, we need an overall understanding of the process to improve the reactivity. First, the pH near the cathode interface greatly impacts the reaction pathways and the formation of certain intermediates. The generated OH^- during the CO_2RR process cannot be immediately transferred to the bulk electrolyte resulting in the pH in the vicinity of the cathode being much higher than that in the bulk electrolyte [68–70]. Ma et al. [71] reported a simple method to determine the local pH experimenting in GDE-based high-rate CO electroreduction. They found that a high local pH facilitated the formation of C_2 products. Therefore, we can add buffering agents, such as KHCO_3 and phosphate, to the electrolyte to reduce the C_2 product and facilitate the formation of CH_4 . It is well-known that CO_2 in water is in acid-base multiequilibrium: $\text{CO}_2 + \text{H}_2\text{O} + \text{OH}^- \rightleftharpoons \text{HCO}_3^- + \text{H}_2\text{O} \rightleftharpoons \text{H}_2\text{CO}_3 + \text{OH}^-$. Higher local pH values would decrease the CO_2 concentration near the interface of the cathode, resulting in the slow kinetics of CO_2RR [72]. A higher pH also decreases the concentration of the H^* intermediate [73]. According to the Langmuir–Hinshelwood mechanism, this will inhibit the formation of CH_4 . Thus, it is critical to investigate the role of the electrolyte on electrochemical CO_2RR .

In addition to the pH effect, hydrated cations can also affect the interfacial interactions occurring at the surface [74–76]. First, hydrated alkali metal cations can serve as a buffer to offset an elevated pH and reduced CO_2 concentration in the vicinity of the cathode. The buffering capacity follows the order of $\text{Cs}^+ > \text{Rb}^+ > \text{K}^+ > \text{Na}^+ > \text{Li}^+$ [77]. According to Chen’s group, the intermediates are stabilized by the electric double-layer (EDL) field formed across the Helmholtz layer via the adsorbate dipole-field interaction, which can be

adjusted by changing M^+ at the interface [78]. Additionally, Koper et al. [79] found that a CO_2 reduction does not occur in the absence of metal cations in the solution. Based on this phenomenon, they proposed that metal cations' main role is stabilizing critical carbon dioxide intermediates. This remarkable observation extends to other common catalysts as well.

3.2. CO_2 Reduction in Non-Aqueous Electrolytes

Nonaqueous electrolytes can be categorized into three distinct types: ionic liquids (molten salts that are composed of organic cations and organic/inorganic anions), organic liquids (such as acetonitrile, methanol, and dimethyl sulfoxide), and mixed solutions of the two. [80]. Non-aqueous electrolytes usually have a higher CO_2 solubility. In methanol electrolytes, the CO_2 solubility is five times higher than that in water at room temperature [81]. Additionally, the absence of proton donors in non-aqueous electrolytes creates an environment that depresses the hydrogen evolution reaction (HER) during electrochemical reactions [82]. Furthermore, due to the variety of non-aqueous electrolytes, we can obtain specific products of CO_2RR by modifying the electrolyte [80]. In the realm of non-aqueous electrolytes, the electrochemical reduction of CO_2 is commonly believed to follow a series of pathways. Initially, CO_2 is activated to create the $CO_2^{\bullet-}$ anion radical, which is deemed the rate-limiting step. Subsequently, two $CO_2^{\bullet-}$ radicals dimerize to produce oxalate, or a disproportionation reaction between $CO_2^{\bullet-}$ and CO_2 generates CO and CO_3^{2-} . Lastly, in the presence of trace amounts of H_2O , $CO_2^{\bullet-}$ can be protonated to form HCOOH or dissociated to produce CO and OH^- [83].

Despite their numerous advantages, the capital cost of non-aqueous electrolytes is much higher than aqueous electrolytes. Additionally, due to the complex structure of non-aqueous electrolytes, the reaction mechanisms remain poorly understood. Hence, a significant amount of further research is necessary before non-aqueous electrolytes can be effectively implemented in industrial applications [84].

4. Progress in the Design of Catalysts for CO_2 Electroreduction to CH_4

In this section, we presented a range of state-of-the-art catalysts and their corresponding construction strategies in a highly informative manner. In order to facilitate the comprehension and applicability of the presented results, illustrative examples were provided in each section, which serves to provide an intuitive understanding of the catalyst construction process. Additionally, it is noteworthy that certain catalysts displayed exceptional electrocatalytic performances, thus highlighting their potential for further exploration and development. Some of the catalysts and their performers are summarized in Table 2.

Table 2. Some catalysts for the heterogeneous electrocatalysis of carbon dioxide to methane.

Catalyst	Electrolyte	Current Density ($mA\ cm^{-2}$)	Applied Potential (V) vs. RHE	CH_4 FE	Ref.
FeSA	1 M $KHCO_3$	200	−1.1	64%	[85]
Cu-CDS	0.5 M $KHCO_3$	40	−1.14~−1.64	78%	[86]
$Cu_{68}Ag_{32}$ nanowire	0.5 M $KHCO_3$	80	−1.17	60%	[87]
MCH-3	1 M KHO	398.1	−1.0	76.7%	[88]
Cu-based cMOF	1 M KOH	162.4	−0.9	80%	[89]
Zn-MNC	1 M $KHCO_3$	31.8	−1.8	85%	[90]
n-Cu/C	0.1 M $NaHCO_3$	-	−1.35	80%	[91]
Cu NW	0.1 M $KHCO_3$	-	−1.25	55%	[92]
Cu–Bi NPs	0.5 M $KHCO_3$	37.2	−1.2	70.6%	[93]
NNU-33(H)	1 M KOH	391.79	−0.9	82%	[94]
Cu^{2+} SA on CeO_2	1 M KOH	200	−0.82	65%	[95]
CoPc@Zn-N-C	1 M KOH	44.3 ± 7.3	−1.24	$18.3 \pm 1.7\%$	[96]
Ag@ Cu_2O -6.4	1 M KOH	178 ± 5	−1.2	$74 \pm 2\%$	[97]

4.1. Catalyst-Structure Engineering

In heterogeneous catalysis, the catalyst's structure impacts the product distribution of electrocatalyzed CO₂ [98–101]. This section focuses on summarizing the different structures of the catalysts, mainly including nanostructured, porous, and single-atom catalysts.

4.1.1. Nanostructured Catalysts

At present, the nano-Cu electrode has been widely studied and used to improve the selectivity and energy efficiency of CO₂RR for CH₄ formations [102,103]. The reactivity of CO₂RR for CH₄ formations over nanostructured Cu is affected by numerous parameters, such as size, coordinated sites, and morphology [104–106]. When the size of nanoparticles decreases, the radius decreases, which results in the increase in ratio of surface to bulk atoms increasing and a decrease in the average coordination of surface atoms. This phenomenon can also be called the activity–selectivity–size relationship [107]. For example, Peter et al. [108] constructed a series of sizes of Cu nanoparticles (Cu NPs) (diameter: 1.2~20.3 nm) (Figure 3A,B). They found that the catalytic activity and selectivity for H₂ and CO products were dramatically increased with the decrease in Cu NP sizes, meaning that the formation of CH₄ was inhibited, in particular when the size of Cu NPs was less than 5 nm (Figure 3C,D). In contrast, the bulk Cu catalysts produced CH₄ as the primary hydrocarbon product from CO₂RR. Buonsanti et al. [109] studied Cu nanocubes (Cu NC) with 24, 44, and 63 nm edge lengths afforded by colloidal chemistry (Figure 3E). As shown in Figure 3F, the cube with a 44 nm edge length has the highest selectivity for CO₂RR at 80%. The surface-atom-density statistical analysis indicated that the edge sites played a key role in the formation of CO₂RR. Although Cu NCs did not possess a high selectivity for the CH₄ formation, it was observed that the size significantly affected the reactivity of the nanostructured catalysts. As shown in Figure 3G,H, a Cu nanowire (Cu NW) catalyst was reported by Yang et al., and such catalysts exhibit high CH₄ selectivity, reaching a CH₄ FE of 55% at –1.25 V vs. RHE (Figure 3I–L) [92]. To further study the effect of the morphology of Cu NW on hydrocarbon selectivity, they wrapped the wires with graphene oxide to keep the morphology stable. It was surprising that the selectivity presented no significant change, indicating that hydrocarbon selectivity is sensitive to the morphology of the catalysts.

As the aforementioned nanostructured Cu elements were not supported by any substrate, the particles could easily aggregate during the electrochemical reaction. The nanostructures supported on substrates also received great attention for their superior performance in electrocatalysts [110,111]. As shown in Figure 4A–D, Alivisatos et al. [91] reported a catalyst that Cu nanoparticles supported on glassy carbon (n-Cu/C) capped with tetracyclphosphonate. The catalyst achieved a methanation current density 4 times higher than the pure Cu foil electrode, and its average CH₄ FE was 80% during the process of extended electrolysis, which is one of the highest CH₄ FE values for room-temperature methanation ever reported (Figure 4E–H). The author proposed that graphene may contribute to lowering the energy barrier of the key step by modifying the electron properties of the anchored Cu nanoparticles due to graphene's unique electronic and physical properties. Additionally, it is easier to increase the Cu–Cu distance on n-Cu/C than that on Cu (111) when the CHO* species is formed on the Cu nanoparticle surface [112]. However, they found that Cu particles supported on glassy carbon can grow during the reaction process, which may be attributed to a combination of particle coalescence and dissolution–redeposition during the electrochemical reaction (Figure 4C,D). The growth of Cu particles impairs the reactivity of the catalyst. Therefore, we need to find strategies to further improve the stability of this catalyst.

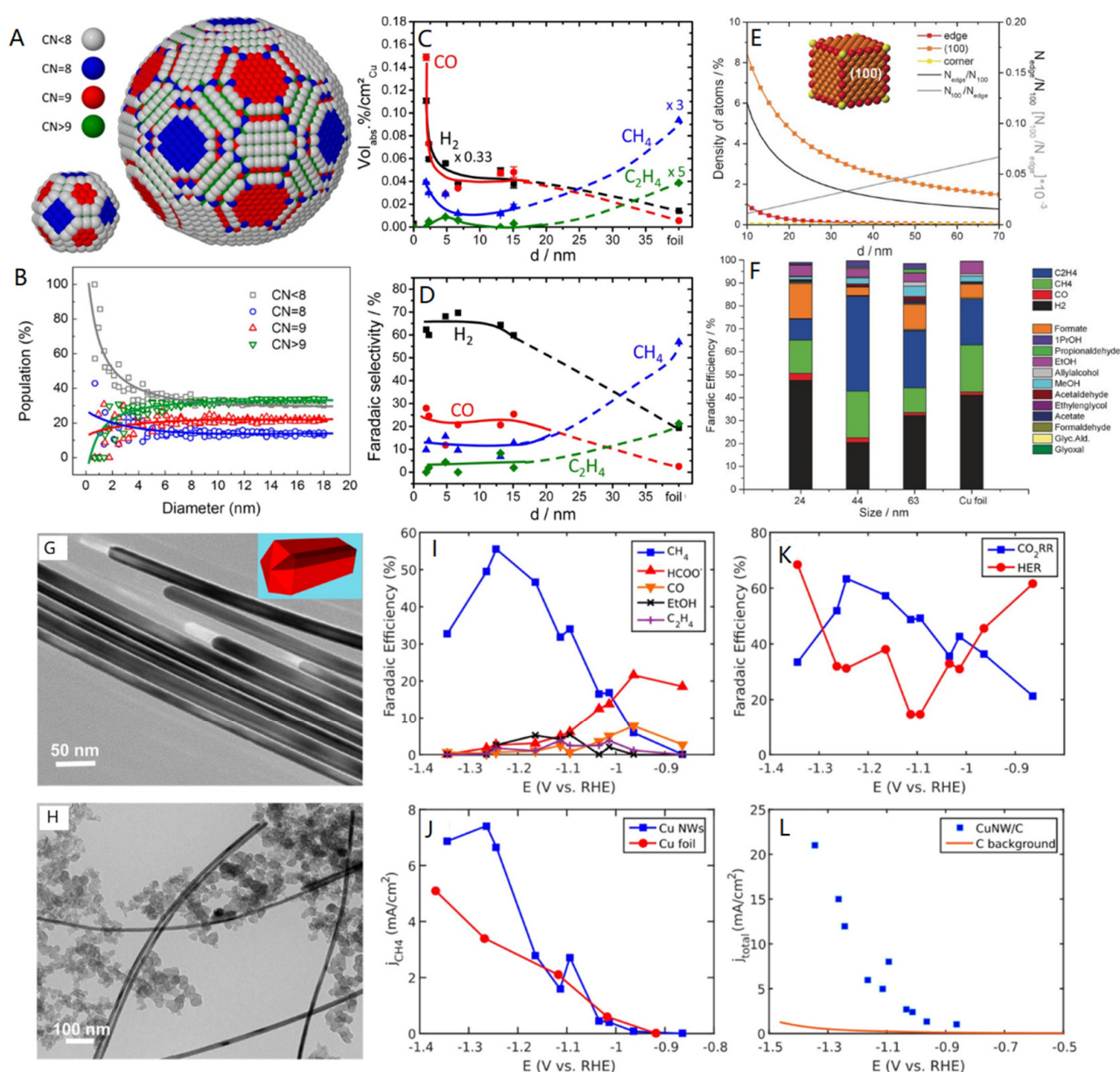


Figure 3. (A) Models of spherical Cu NPs with 2.2 and 6.9 nm diameters and the quantity of Cu atoms with different coordination numbers; (B) population (relative ratio) of surface atoms with a specific CN as a function of particle diameter; (C) the composition of gaseous-reaction products; (D) FE of reaction products during CO₂ electroreduction are a function of the diameter of Cu NPs (reproduced with permission from Ref. [108]); (E) density of adsorption sites in Cu NC cubes to the edge length; (F) FE of each product in Cu NC cubes and Cu foil at -1.1 V vs. RHE (reproduced with permission from Ref. [109]); (G) TEM image of bare wires (the insert shows the 5-fold twinned structure, showing a high proportion of low-coordination edge sites); (H) TEM micrograph of Cu NWs loaded on carbon; (I–L) Cu NW initial electrocatalytic activity and selectivity. Reproduced with permission from Ref. [92].

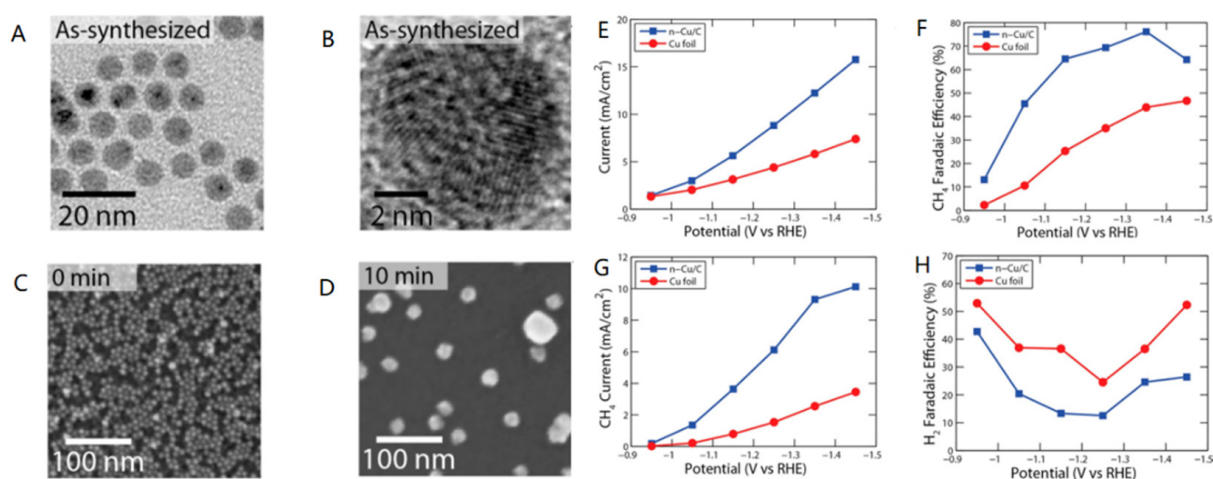


Figure 4. TEM images: (A) low magnification; (B) high-magnification and SEM images of (C) as-synthesized and (D) evolution of Cu NP supported on glassy carbon after 10 min. (E–H) Potential (V vs. RHE) dependence on: (E) current (mA cm^{-2}); (F) CH₄ FE; (G) CH₄ current (mA cm^{-2}); (H) H₂ FE of n-Cu/C and Cu foils. Reproduced with permission from Ref. [31].

4.1.2. Porous Catalysts

Porous catalysts have attracted considerable attention, recently, because of their large specific surface areas, high density of surface-active sites, efficient mass transfer, and optimization of intrinsic activity [113–116]. In addition, nanopores provide a low coordination position for the reaction [117]. The selectivity of porous catalysts can be changed by increasing the residence time of the intermediates [104]. Because of this characteristic, various porous catalysts for the selective catalysis of CO₂ to CH₄ and relevant strategies have been developed [118]. Wen et al. [88] reported a perfluorinated covalent triazine framework (FN-CTF-400) that shows an astonishingly selective catalysis of CO₂ to CH₄ with a dominant competitive advantage over HER. As shown in Figure 5A–F, the CH₄ FE value is about 78.7% at potentials between -0.4 and -0.6 V vs. RHE, and what is even more impressive is that the CH₄ FE value of FN-CTF 400 can reach 99.3% at the potential between -0.7 and -0.9 V vs. RHE. However, when the potential increases above -1.0 V, the efficiency gradually decreases to 65%. According to the DFT calculations, the high-selectivity depends on the doping fluorine, which regulates the activity of N, making it more conducive to CH₄ production (Figure 5G–K). Wen et al.’s outstanding work provides important guidance for designing carbon dioxide electroreduction strategies for more favored materials.

MOF (metal organic framework) and COF (covalent organic framework) are two kinds of crystalline porous materials with a periodic network structure. They have recently been widely used in electrochemistry, especially as an energy-related electrocatalyst for their unique structure. Lan et al. [89] synthesized and studied a series of honeycomb-like porous crystalline hetero-electrocatalysts. This is a core–shell-structured material with HMUIO-66-NH₂ as the core (HM stands for honeycomb-like MOF) and COF-366-Cu as the shell (constructed by tetra(*p*-aminophenyl)porphyrin (Cu-TAPP) and 2,5-dihydroxyterephthalaldehyde (DHA)). MCH-X (X = 1–4) (MCH-X, X = 1–4, X: different MOFs doses in MCH synthesis) was synthesized by adjusting the different amounts of HMUIO-66-NH₂ in the COF synthesis system. Among them, MCH-3 presented the best performance with an excellent current density at $-398.1 \text{ mA cm}^{-2}$ and superior CH₄ FE as 76.7% at -1.0 V vs. RHE. Rich, open channels of the catalysts facilitated the CO₂ adsorption/activation and conversion to CH₄ processes. Lan’s group also [119] reported a Cu-based conductive metal organic framework (cMOF) that combines electrical conductivity with the porosity of MOF. It is composed of highly conjugated graphene ligands (dibenzo-[*g,p*]chrysene-2,3,6,7,10,11,14,15-octaol, 8OH-DBC) and Cu ions. Highly conjugated organic ligands endow Cu-DBC with unique redox properties and electrical conductivity (Figure 6A). CH₄ FE exhibits up to 80% (Figure 6B,C) accompanied by a

partial current density of $+162.4 \text{ mA cm}^{-2}$ at a low reduction potential of -0.9 V vs. RHE . The abundant and uniformly distributed Cu–O₄ sites greatly contributed to the effective ERC-to-CH₄ process with high selectivity.

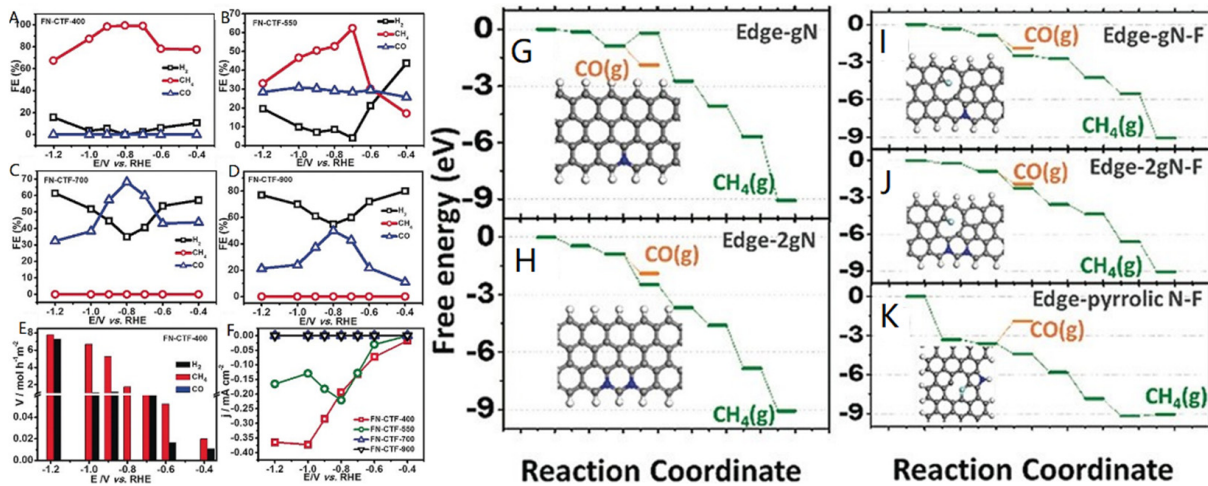


Figure 5. Potential of electrodes' dependence on CH₄, CO, and H₂ FE production: (A) FN-CTF-400, (B) FN-CTF-550, (C) FN-CTF-700, and (D) FN-CTF-900; (E) hydrogen, carbon monoxide, and methane yields of FN-CTF-400 at different applied potentials; (F) corresponds to the current density generated by CH₄ on the FN-CTF sample set; (G–K) reaction models of active sites in N-doped and N- and F-co-doped structures. C: gray, H: white, N: blue, F: cyan. As for the FED, green paths: CO and orange paths: CH₄. Reproduced with permission from Ref. [88].

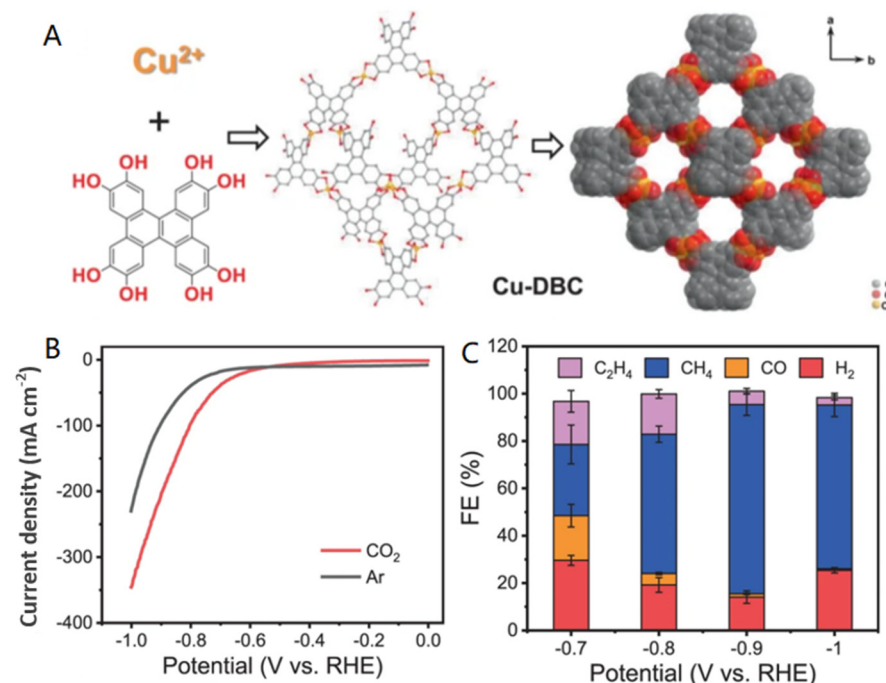


Figure 6. (A) The structure of Cu-based conductive metal organic framework; (B) polarization curves recorded in CO₂ and Ar atmospheres; (C) FEs of ERC products at different applied potentials. Reproduced with permission from Ref. [39].

Although many achievements have been made in the research and application of porous catalysts, the role of the pore size in the catalytic process is still rarely reported. As the size of the catalysts can affect the mass transfer and density of the activity site, we need to study the role of pore size further.

4.1.3. Single-Atom Catalysts

Single-atom catalysts (SACs), in which single metal atoms are anchored to the support, have recently attracted considerable attention [120–123]. The active sites of SACs are isolated metals coordinated by pyridine/pyrrole nitrogen atoms, carbon atoms, or other substrates [124]. The highly isolated active sites of SACs can effectively inhibit the C–C coupling process. Therefore, it can promote the generation of CH₄. Additionally, SACs provide the economical, efficient utilization of precious-metal catalysts and open up a broad new field for optimizing the selectivity and activity of various reactions due to their uniform monoatomic dispersions and clear structures [125]. For example, when using single-atom Cu substitute Ce on the CeO₂(110) surface, three oxygen vacancies around each Cu site are steadily concentrated, producing efficient carbon dioxide adsorption and activating catalytic centers [126].

Recently, Zhu et al. [86] reported that Cu-embedded carbon dots (Cu-CDS) prepared by calcining Na₂ [Cu (EDTA)] 2H₂O at 250 °C (the lowest carbonization temperature) converts the carbon-containing molecular complex into solid Cu-CDS, which retains the SAC coordination environment (Figure 7A). The electrocatalytic activity of the catalyst was tested and the results showed that the FE of methane was as high as 78% at the potential of 1.14~1.64 V. Among carbon dioxide-reduction products, 99% were CH₄ (Figure 7B–G). The DFT calculations indicate that HER is well-inhibited by CuN₂O₂ on the catalyst, which accounts for the high selectivity of CO₂RR for CH₄ formation. The easy preparation of this catalyst allows them to have a broader range of application scenarios.

Edward et al. [85] reported a metal-supported monatomic catalytic center. They prepared gas diffusion electrodes (GDEs) by depositing sputtered Cu on a polytetrafluoroethylene (PTFE) substrate and then assembled iron phthalocyanine (FePc) on the Cu surface. By changing the size of the Fe cluster, they found that the affinity of the Fe atom for *CO increased when the size of the Fe cluster decreased. When it decreased to a single site, the affinity for *CO reached the highest point (Figure 8B). As shown in Figure 8C, *CO is transferred to the Fe atom from Cu near the bridge and top sites. The main product of Cu supporting the iron monatomic catalyst was CH₄. When the current density was 200 mA cm⁻², CH₄ FE can reach the maximum of 64%, which is much higher than that on bare Cu catalysts with CH₄ FE as low as 2%. It may be that the C–C coupling is unfavorable to FeSA compared to the surface of bare Cu; therefore, *CO is more readily hydrogenated to *COH on the Fe site of Cu-FeSA than *CHO when a solvation contribution is present (Figure 8D,E).

Xin et al. [90] reported the electrocatalysis of single Zn atoms supported on N-doped carbon (Zn-MNC) (Figure 9A,B), which was demonstrated by normalized X-ray absorption near-edge structure (XANES) curves, the Fourier transform (FT) k²-weighted extended X-ray absorption fine-structure (EXAFS) spectrum, X-ray absorption spectroscopy (XAS), and X-ray photoelectron spectroscopy (XPS) shown in Figure 9C–F. Compared with the saturated calomel electrode, the catalyst showed a high CH₄ FE of 85% with a partial current density of –31.8 mA cm⁻² at a potential of –1.8 V. Zn-MNC presented a significant stability improvement since no apparent current drop and great FE fluctuation were observed after 35 h of the electrochemical-reduction reaction (Figure 9G–J). The theoretical calculation shows that a single zinc atom hinders the formation of CO to a large extent, but promotes the formation of CH₄. Although the partial current density was low, this proved the feasibility of copper-free elements catalyzing CO₂ to hydrocarbons.

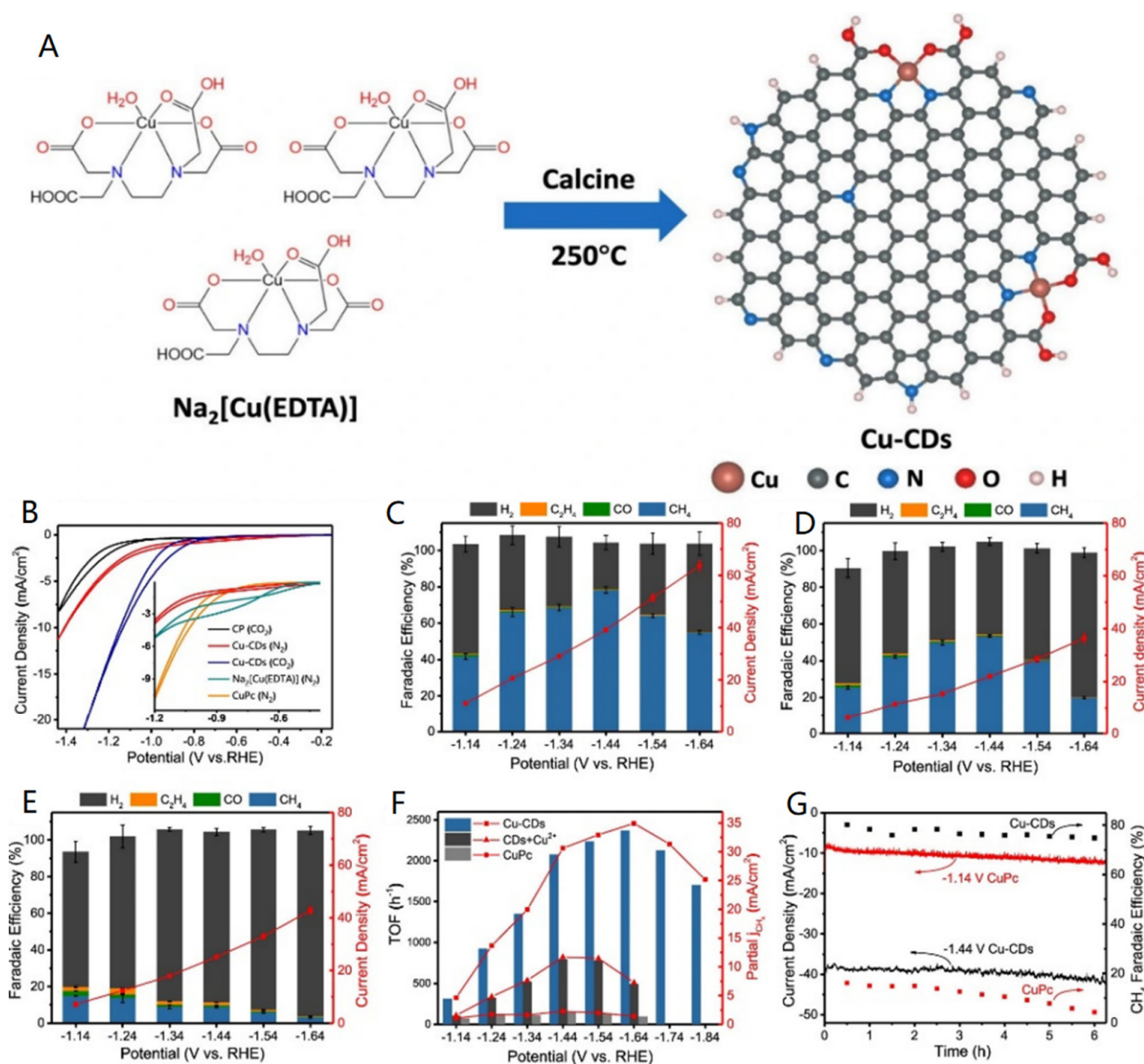


Figure 7. (A) Scheme of low-temperature roasting process of Cu–CD catalyst; (B) CV curves for CP (bare carbon paper), CuPc, Na₂[Cu (EDTA)], and Cu–CDs. The dependence of FE and current density (based on geometric surface area) on the applied potentials of (C) Cu–CDs, (D) CDs + Cu²⁺, and (E) CuPc. (F) The CH₄ partial current density patterns and TOF spectra of Cu–CDs, CDs + Cu²⁺, and CuPc were studied at different potentials; (G) stability tests for Cu–CDs and CuPc at their highest ERC FE potentials. Reproduced with permission from Ref. [86].

To achieve large-scale industrial applications, it is necessary to further improve the stability. Increasing the conversion rate is also an indispensable technique. In addition, if a new type of SAC-preparation method can be developed to improve the preparation process of SACs and simplify their production process, it is also expected to significantly reduce the production cost of SACs [43].

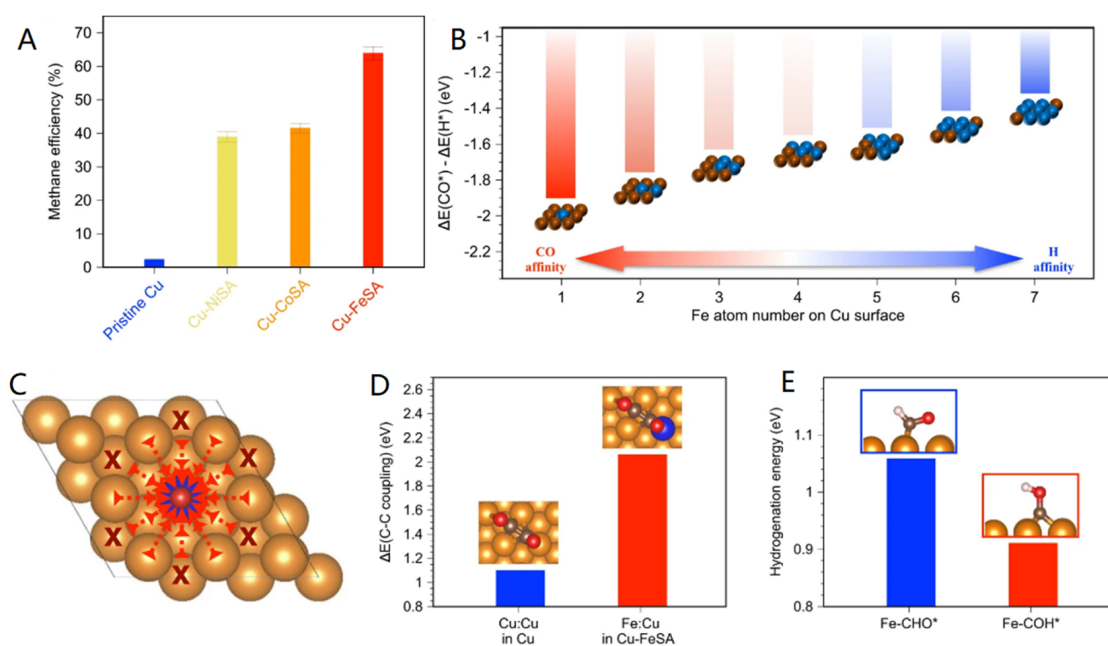


Figure 8. (A) Catalytic CH₄ activities of pristine Cu vs. various single-atom-anchored Cu catalysts for CO₂ reduction reaction; (B) adsorption energies of *H and *CO are affected by the size of Fe on the Cu surface; (C) diagram of *CO transition: the arrow indicates the transition path and the crosshair indicates the fixed *CO-adsorption site; (D) coupling energies of pure Cu and Cu-FeSA; (E) hydrogenation energy of methanogenic intermediates on Fe center in Cu-FeSA. Reproduced with permission from Ref. [85].

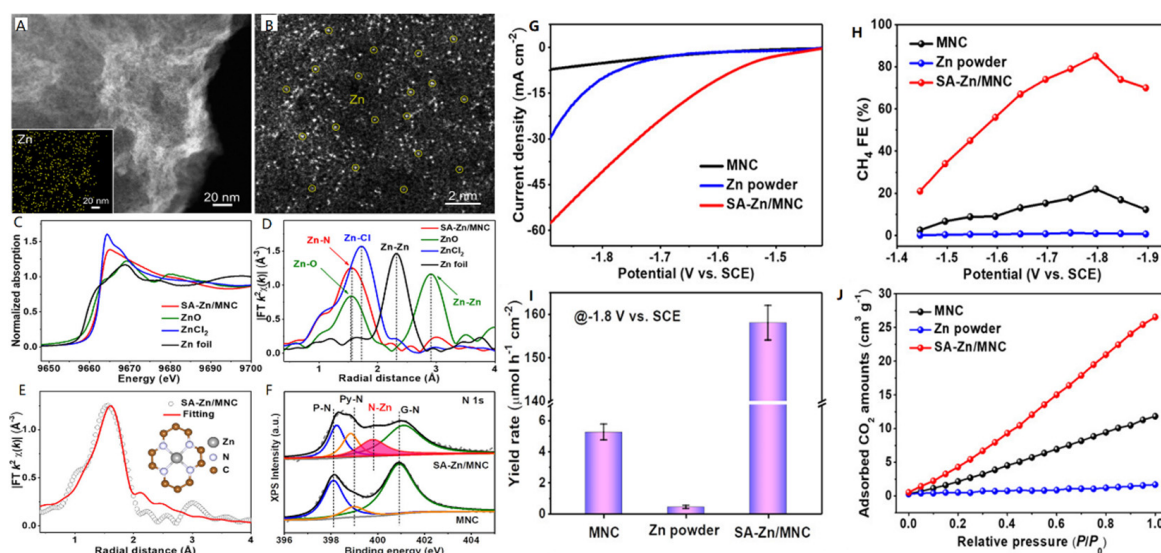


Figure 9. (A) HAADF-STEM image of an SA-Zn/MNC inset: EDS mapping of Zn. (B) Atomic-resolution HAADF-STEM image with some Zn atoms highlighted by yellow circles. (C) XANES and (D) FT-EXAFS spectra. (E) FT-EXAFS. (F) XPS. (G) Current density, (H) FE, (I) yield rate, (J) and adsorbed CO₂ quantities on MNC, Zn powder, and SA-Zn/MNC, respectively. Reproduced with permission from Ref. [90].

4.2. Catalyst Component Engineering

In addition to the previously summarized strategies for the structural part of the catalyst, we observed that there were also numerous works devoted to tuning the catalyst composition as a way to improve product selectivity. Therefore, this section summarizes the relevant work in terms of alloy, oxidation-state Cu-containing, and tandem.

4.2.1. Alloy Catalysts

According to the previous literature, Cu is the only metal that can catalyze CO₂RR to efficient amounts of hydrocarbons and oxygenates due to the suitable adsorption strength of *CO [127,128]. However, it is greatly hindered by poor selectivity and a high overpotential to eliminate the CO from CHO energy barriers on the pure-Cu crystal surface, which is unacceptable for industry-scale applications. To tackle this problem, numerous efforts have been devoted to developing Cu-alloy catalysts [129–131].

Alloying Cu with a foreign metal can improve its electrocatalytic performance, compared to single-metal Cu catalysts, by imparting some unique properties to them, including electronic (changing the electronic structure of the host metal by adding different metals) and geometric (changing the atomic arrangement of active sites) effect [132–134]. According to the d-band model, the electron effect can change the binding strength of intermediates adsorbed on the surface [135]. Additionally, geometric effects can adjust the binding energy of the intermediates and catalysts, hence tuning their catalytic activities [87]. We can also create bifunctional active centers in which neighboring metals play different catalytic roles, in addition to simply changing the numbers or configurations of specific atoms in the ensemble. The introduction of foreign metals into Cu also changes its surface chemistry, thus changing the distribution of the products [136]. These Cu-alloy catalysts also show significant reactivity behavior to CO₂RR for CH₄ formation, outperforming pure metals [130].

Goddard et al. [93] prepared Cu–Bi NPs (Figure 10A–D) through a facile, one-step method, which presented higher activity and selectivity to CH₄. The Cu₇Bi₁ NPs presented a CH₄ FE as high as 70.6% at –1.2 V vs. RHE, which is almost 25 times that of Cu NPs (Figure 10E–J). DFT calculations showed that the addition of bismuth significantly reduced the energy formation of the potential energy-determining step (PDS) for the electrocatalysis of CO₂ to CH₄. The highly electropositive bismuth absorbed an electron from Cu, causing the Cu to be partially oxidized, which is the active center where CO₂RR is most likely to be converted into CH₄.

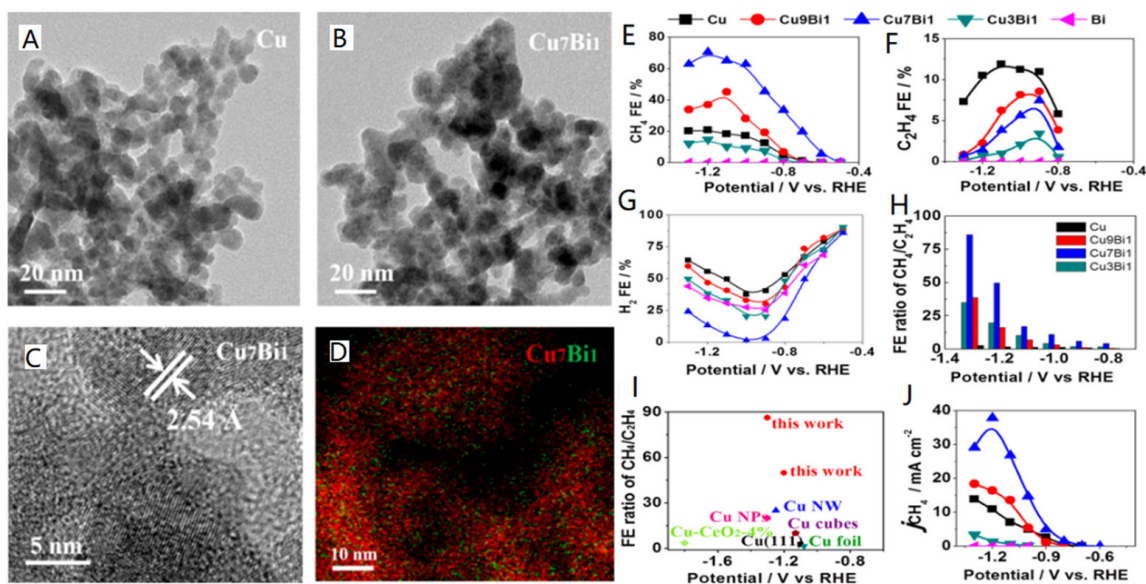


Figure 10. TEM images of (A) Cu and (B) Cu₇Bi₁ NPs; (C) HRTEM image and (D) EDX mapping of Cu₇Bi₁ NPs. CO₂ electroreduction performance of the synthesized NPs: (E) FE of CH₄; (F) FE of C₂H₄; (G) FE of H₂; (H) FE ratio of CH₄/C₂H₄; (I) comparison of present work with previously reported CH₄ selectivity; (J) partial current densities of CH₄. Reproduced with permission from Ref. [93].

Lee et al. [137] studied a bimetallic Cu/Ag-layered catalyst for eliminating the geometric effect from the electrocatalytic performance by varying the thickness of the Ag layer (Figure 11A). The optimized Cu/Ag-layered catalyst exhibited bifunctional catalytic characteristics that preferentially produced CO (FE = 89.1%) at -0.8 vs. RHE and had a high-selectivity value of CH₄ (FE = 65.3%) at -1.2 vs. RHE (Figure 11 B). The silver atoms on the surface of Cu reduced the charge density by forming additional bonds with Cu. With the increase in the thickness of the silver layer, the d-state center gradually shifted down from the Fermi level, which produced weak CO-binding energy on the surface.

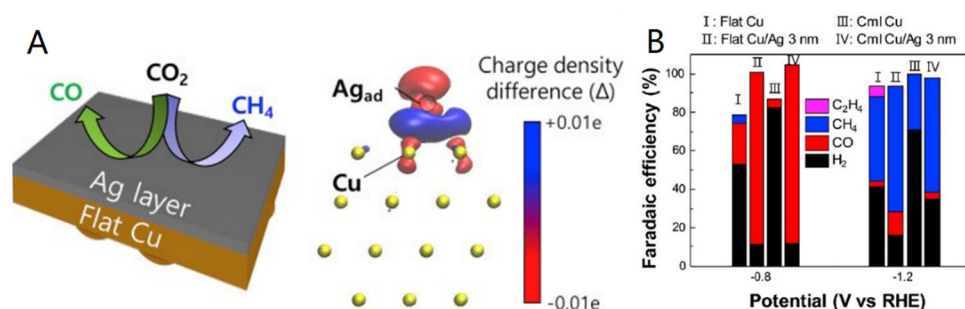


Figure 11. (A) Cu/Ag-layered catalyst for eliminating the geometric effect from the electrocatalytic performance by varying the thickness of the Ag layer; (B) measured FE at -0.8 and -1.2 V vs. RHE. Reproduced with permission from Ref. [137].

4.2.2. Oxidation-State Cu-Containing Catalysts

Introducing Cu^{+} to the surface of Cu catalysts has been suggested as an active site for CO₂RR [138]. Studies have shown that the stable presence of Cu⁺ can improve the activity of CO₂RR for CH₄ formation [139]. However, in the process of an electrochemical reaction, Cu⁺ can be easily reduced to Cu due to its instability. Therefore, the oxidation state of Cu may be of great significance in improving its catalytic activity. As shown in Figure 12A, Lan and coworkers [94] synthesized two stable Cu⁺ coordination polymer (NNU-32 and NNU-33(S) (S = sulfate radical)) catalysts, which showed high selectivity for the electrocatalytic conversion of CO₂ to CH₄. NNU-33(H) created an impressive CH₄ FE amount of 82% at -0.9 V vs. RHE with a partial current of 391 mA cm⁻², which was one of the best-reported Cu-based catalysts for CO₂RR to produce CH₄ (Figure 12B,C). This may account for the greatly enhanced coprophilic interaction observed in NNU-33 (H) and the in situ OH⁻ substitution of SO₄²⁻ inherent in the molecule, which decreased the Gibbs free energy of PDS (*H₂COOH → *OCH₂). The DFT further confirmed this result. The *CO-adsorption energy of Cu-based catalysts increased monotonously with the increase in the oxidation state [136]. Therefore, Cu²⁺ may have a stronger adsorption capacity for *CO. Qiao et al. [95] incorporated Cu²⁺ ions into a CeO₂ matrix to obtain stabilizing Cu²⁺ ions. The appearance of CeO²⁻ was demonstrated by in situ Raman spectroscopy, which showed a peak at 560 cm⁻¹ originating from the electrochemical reduction of Ce⁴⁺ to Ce³⁺, indirectly demonstrating the stable presence of Cu⁺ (Figure 12D,E). The performance was evaluated in the flow reactor for over 6 h, and the average CH₄ FE was about 65% at a constant potential of -1.4 V vs. RHE (Figure 12F-I). The DFT calculation demonstrated that stable Cu²⁺ active sites can significantly improve the initial adsorption of CO and promote the hydrogenation of *CO to *OCH₃. Both of the abovementioned catalysts showed excellent catalytic performances. It can be seen that maintaining oxidized copper is a good idea for designing catalysts.

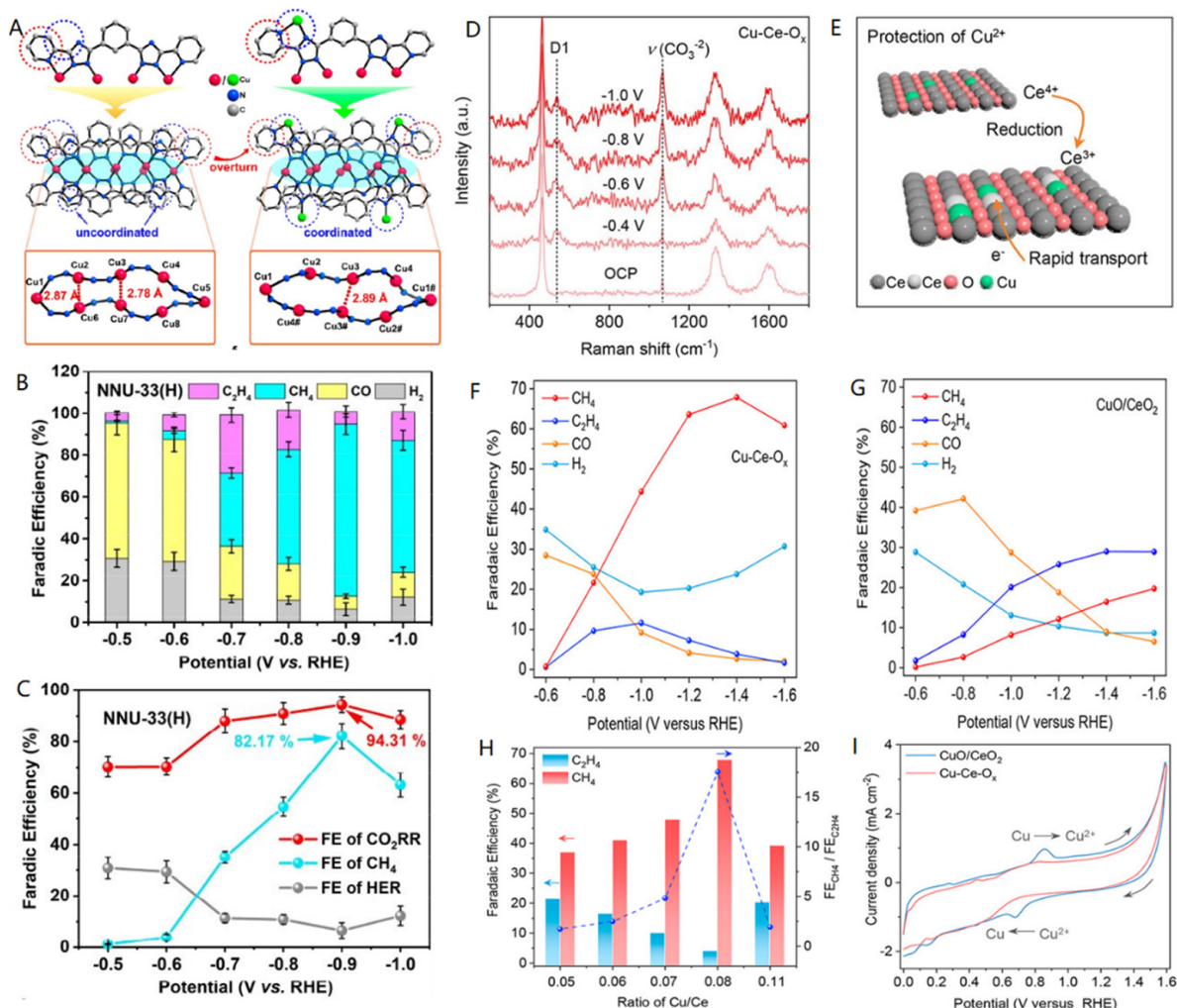


Figure 12. (A) The crystal structures of NNU-32 and NNU-33(S): NNU-32: coordinated Cu^+ ions in NNU-32 (left), NNU-33(S) (right): coordinated Cu^+ ions in NNU-33(S); (B) NNU-33(H) FE of H_2 , CO , CH_4 , and C_2H_4 ; (C) comparison of FE to HER, total CO_2RR , and CH_4 conversion to NNU-33(H); (D) in situ Raman spectra for Cu-Ce-Ox collected at different potentials, indicating the existence of Cu^+ . Reproduced with permission from Ref. [94]; (E) self-sacrificing mechanism to protect Cu^{2+} ; CRR performance of various samples (F,G); FEs for CRR products at different potentials. (H) FE_{CH_4} of Cu-Ce-Ox catalysts corrected by IR compared with that of other reported Cu-based catalysts; (I) ratio of FE_{CH_4} to $\text{FE}_{\text{C}_2\text{H}_4}$ of CuO/CeO₂ and Cu-Ce-Ox. Reproduced with permission from Ref. [95].

4.2.3. Tandem Catalysts

Cu is one of the only catalysts that can further reduce CO to a more value-added hydrocarbon during the CO_2RR . Nevertheless, when CO and CHO are both bound to the same surface, the binding energies follow the linear scaling relationship that limits CO from being reduced further to CHO [56], leading to the disadvantages of high overpotential and low CH_4 FE on the single-component Cu catalyst. On the other hand, it is a promising strategy to convert CO_2 into CO on more efficient catalysts, such as Au and Ag [140,141], and then reduce the CO generated on Cu to break the limitation of the linear scaling relationship of the key intermediates' adsorption of the abovementioned single Cu catalyst and obtain CO_2RR products with a high selectivity and high yield. Based on this principle, numerous tandem catalysts have been developed, and the key factor to be considered in the design of tandem catalysts is how to efficiently transfer CO intermediates from the catalyst that generates CO to Cu.

Recently, Bao and coworkers [96] reported a Cu-free tandem catalyst consisting of cobalt phthalocyanine (CoPc) and zinc–nitrogen–carbon (Zn–N–C) (CoPc@Zn–N–C) that can effectively and electrochemically reduce CO₂ to CH₄. CO₂ is reduced to CO over CoPc, and the generated CO diffuses to Zn–N–C to convert further into CH₄ (Figure 13A,C). Compared with CoPc or Zn–N–C alone, the formation-rate ratios of CH₄ and CO₂ of this tandem catalyst are over 100 times higher (Figure 13B,D,E).

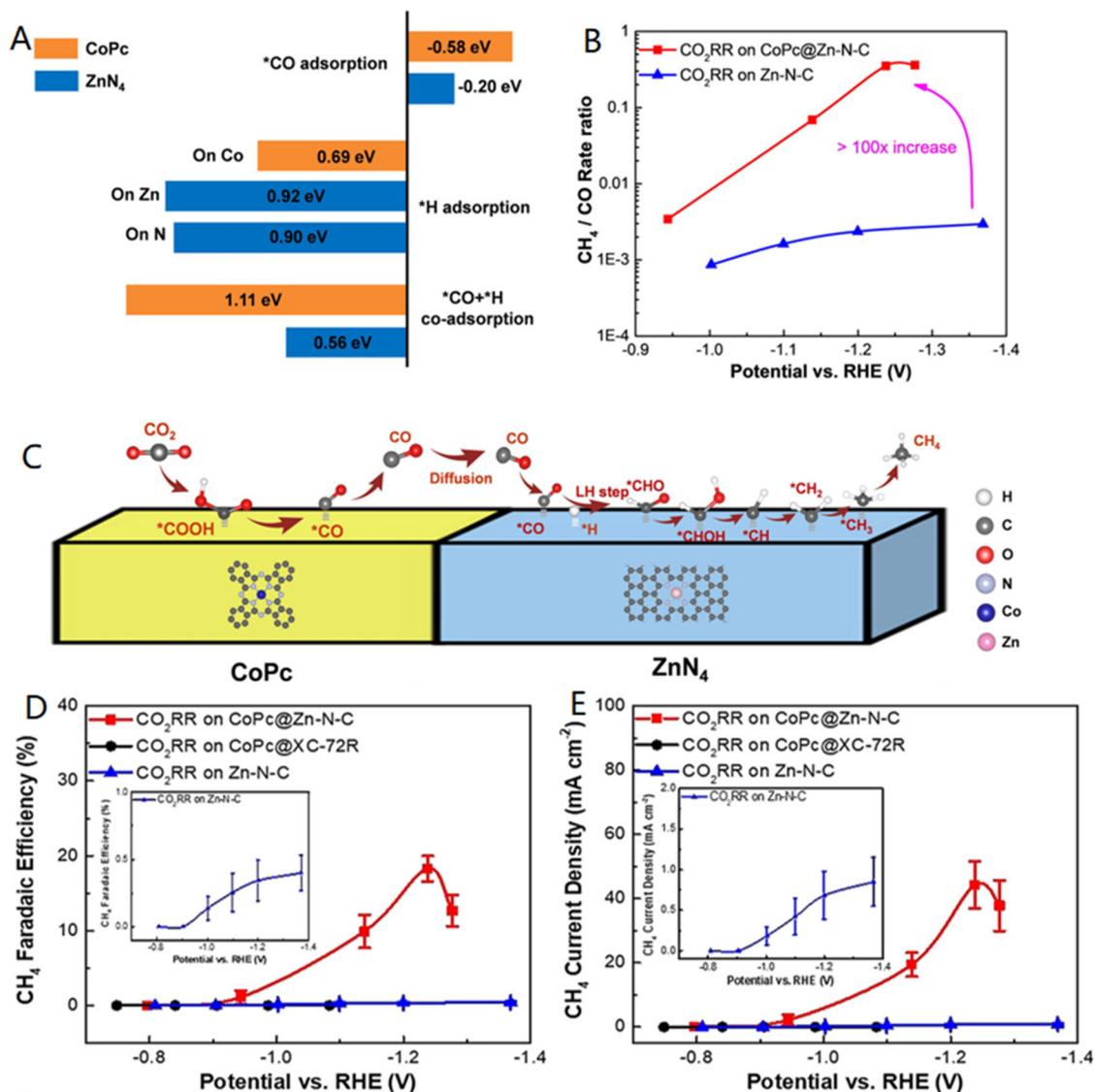


Figure 13. (A) The adsorption energy profiles of *CO, *H, and the co-adsorption of *CO and H* on CoPc and ZnN₄, respectively; (B) CH₄/CO production rate ratio over CoPc@Zn–N–C and Zn–N–C, respectively; (C) reaction mechanism of CO₂RR for CH₄ formation over CoPc@Zn–N–C; (D) CH₄ FE; (E) potential dependence of CH₄ partial current density of CO₂RR. Reproduced with permission from Ref. [96].

Peng et al. [97] constructed a yolk-shell nanocell structure comprising an Ag core and a Cu₂O shell that resembled a tandem nanoreactor (Figure 14A–C). Among them, Ag@Cu₂O-6.4 NCs (6.4 represents the mole ratio of Cu/Ag) exhibited the greatest CH₄ selectivity, achieving a maximum FE value of 74 ± 2% and a high partial current density of 178 ± 5 mA cm⁻² at -1.2 V vs. RHE and CH₄ FE as 72 ± 3% at -1.3V vs. RHE with the local current density continuously increased to 214 ± 9 mA cm⁻² (Figure 14D–E). It is worth noting that the performance was almost the best among the most advanced

CO₂RR catalysts especially used for CH₄ production and met the technical and economic requirements of any commercially feasible CO₂RR catalyst with a current density greater than 100 mA cm⁻². Ag@Cu₂O NCs with different Cu₂O envelope sizes exhibited different product distributions. This was because varying CO fluxes per unit area at the shell resulted in varying CO coverage on the Cu₂O surface, further confirmed by both the experiment and DFT (Figure 14F).

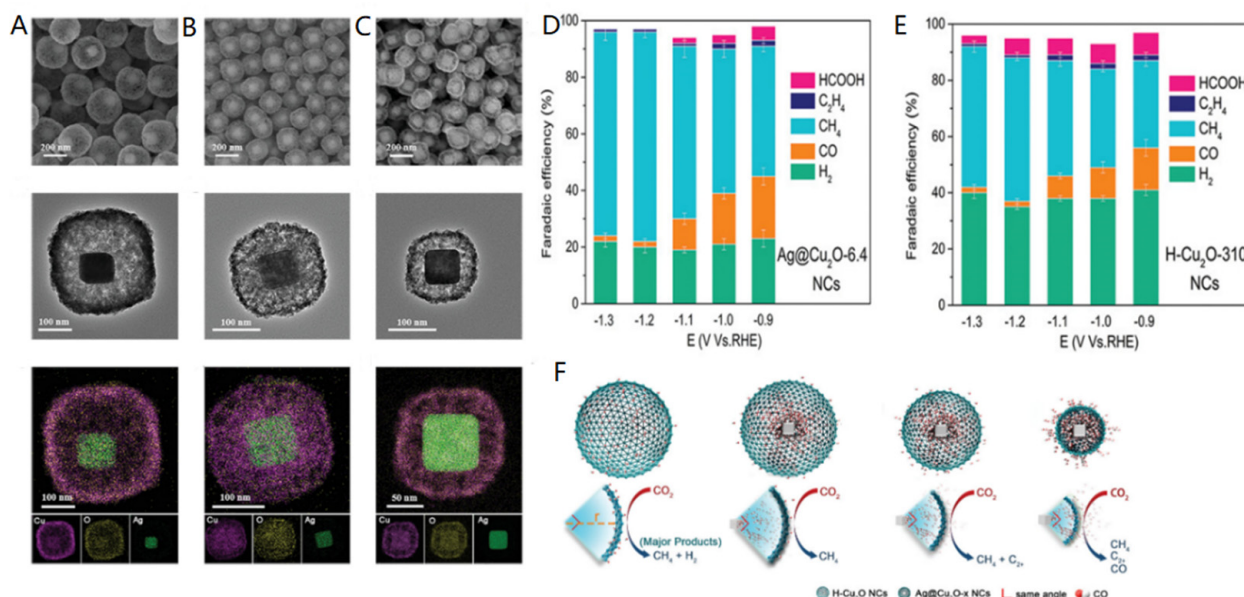


Figure 14. Microstructure of Ag@Cu₂O-*x* nanocells: SEM, TEM, and EDX mapping images of (A) Ag@Cu₂O-6.4 NCs, (B) Ag@Cu₂O-2.9 NCs, and (C) Ag@Cu₂O-1.1 NCs. FE of (D) Ag@Cu₂O-6.4 NCs, (E) H-Cu₂O-310 NCs; (F) schematic diagram shows the CO flux in Ag@Cu₂O-*x* NCs with different outer diameter-Cu envelope sizes and the modulation of the reduced production by the emitted CO molecules from the silver core. Reproduced with permission from Ref. [66].

5. Techno-Economic Analysis and Life Cycle Assessment of Electrochemical CO₂ Reduction to Methane System

Within this section, a concise examination of the techno-economic analysis pertaining to a general process of the conversion of CO₂ to CH₄ via electrochemical means is presented encompassing CO₂ capture, electrochemical conversion, reactant recycling, and product separation. All the prices used here were based on the Chinese market, to date (the exchange rate of USD to CNY is, at present, 6.88, which will fluctuate over time), and did not take into account the impacts of financial factors, such as carbon taxes or credits. Additionally, due to the absence of commercially developed analogs, a comprehensive analysis of a CO₂-reduction process was challenging. Nevertheless, utilizing engineering approximations and making assumptions based on existing technologies can provide valuable insights [142]. We used the net present value (*NPV*) approach to evaluate the feasibility of this technology. The *NPV* was derived through the aggregation of the present values of cash inflows and outflows, which were discounted to the present time using an appropriate discount rate throughout the entire duration of the project or process. If the *NPV* was positive, then the project was considered valuable; if the *NPV* was negative, then the project was considered unprofitable.

$$NPV = \sum_{i=1}^{i=n} \frac{C_i}{(1+r)^i} - C_0$$

where C_0 is the initial investment, C_n is the n year cash flow, i is the year, and r is the discount rate.

Figure 15 provides a comprehensive overview of the CO₂ to ethylene conversion process. The initial step involved the capture of CO₂ from a high partial-pressure stream, such as biogas or industrial flue gas [143–147]. From the information provided by some companies, such as Carbon Clean, the costs of CO₂ capture from industrial flue gas through membrane, pressure swing adsorption, and scrubbers were comparable for large-scale processes, ranging between USD 30–\$0/ton CO₂ [146,148]. However, capturing CO₂ from the air is significantly more expensive, with the cost being 5–10 times more than the aforementioned range, rendering it an unviable approach for this study. The capital cost of installing a CO₂ capture and storage facility with an annual capacity of 100,000 tons at a steel plant is approximately USD 27 million.

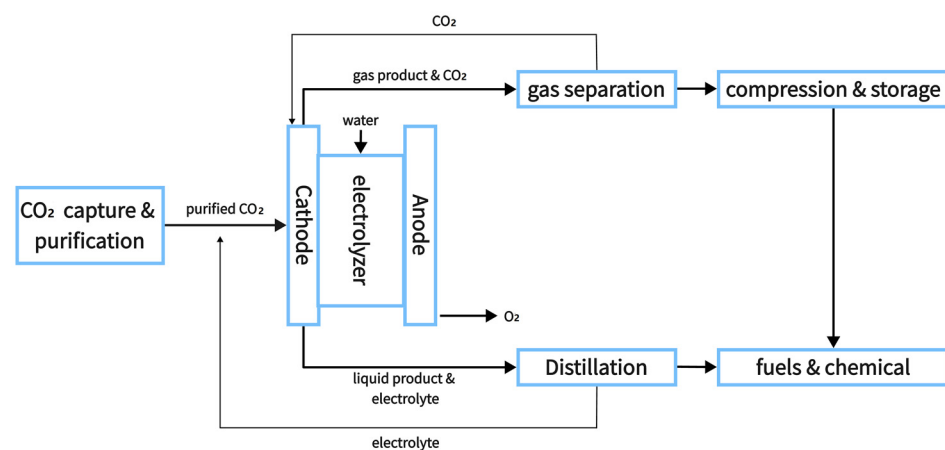


Figure 15. A general CO₂ electrolysis process.

Here, we coupled carbon capture with electrochemical CO₂ conversion to cut off the cost of gas transportation [149]. The subsequent step entailed feeding the captured CO₂ into a high-pressure (10 bar) GDE-based electrolyzer to produce CH₄. It is worth mentioning that the CO₂ feed does not necessitate additional pressurization since CO₂ derived from biogas plants is often available at high pressures. However, determining the distribution of products was challenging, as it was contingent to various factors, such as temperature, pressure, catalyst type and morphology, cell potential, current density, and pH. Despite the uncertainties, this study assumed a fixed FE of 90% for CH₄ and 10% for H₂ at −1.3 V vs. RHE, respectively.

$$P = I \times V \times t = QV$$

$$Q = It = \frac{M_{\text{CO}_2} \times F \times 8}{44 \times FE_{\text{CH}_4}}$$

where P is the power required. The total current, V , is the cell voltage (here, we did not consider the value of oxygen generated by the anode as a compensation without considering the anode voltage). Therefore, based on Section 4, we set the voltage to −1.3 V), FE_{CH_4} fixed as 90%. F is the Faraday constant (96,485.334C).

According to the STATE GRID Corporation of China, we knew that the electrovalency was USD 0.091/(kW·h). Therefore, the capital cost of electric power was USD 4.5 million per year. In order to approximate the capital expenses associated with an electrolyzer system, a typical model of an alkaline water electrolyzer stack was utilized. According to several companies that are involved in alkaline water electrolyzers, such as the China Huadian Corporation, the capital cost we obtained for the stack component was USD 300/KW. Therefore, for a capacity of 100,000 tons, the initial stack cost was USD 20 million. Another important factor was that stability pertains to the gradual deterioration or deactivation of the electrode catalyst and the overall electrochemical cell. Here, we established that the electrode material could work for 8000 h per year and the maintenance cost was 2.5%.

The subsequent step was to separate CH₄ (account for 0.473), H₂ (account for 0.21), and unconventional CO₂ (account for 0.315) (as the conversion of CO₂ was rarely reported, we set the conversion rate as 60%, which can be achieved by a well-designed electrolyzer). Pressure swing adsorption (PSA), membrane, and low-temperature separations are usually applied to gas product separation, [150–152] But achieving a purity level higher than 99% through membrane separation was challenging. Therefore, we opted to employ pressure swing adsorption (PSA) separation as a means of separating methane and hydrogen [153–155]. Technical details can be found in the ref. [156]. According to Augelletti et al. [156], we can obtain a relatively high concentration of methane gas at a low power cost (270 kJ/kg). The proposed methane fee was intended to specifically target the natural gas and petroleum industries and would entail a cost of USD 300 per ton of methane, which is the lowest price for CO₂-reduction products (Table 3). A reference cost of USD 1,990,000 per 1000 m³/h capacity was used [142]. According to the National Energy Administration, the price of hydrogen was USD 5.09 per kilogram.

Table 3. Market prices of CO₂-reduction products. Ref. [142] notice: The data presented in this table are for 2018.

Product	Number of Required Electrons	Market Price (USD/kg)	Normalized Price (USD/electron) × 10 ³	Annual Global Production (Mtonne)
Carbon monoxide (syngas)	2	0.06	0.8	150
Carbon monoxide	2	0.6	8	
Formic acid	2	0.74	16.1	0.6
Methanol	6	0.58	3.1	110
Methane	8	0.18	0.4	250
Ethylene	12	1.3	3	140
Ethanol	12	1	3.8	77
n-Propanol	18	1.43	4.8	0.2

As shown in Table 4, we summarized the capital and operating costs of CO₂ electrolyzers. We briefly examined various parameters, including CO₂, electricity, and selling prices of the final product, which significantly impacted the cost analysis. The financial model does not incorporate the expenses related to sales, labor, and inflation. We observed that, no matter how we optimized the reaction conditions and reduced the costs, we did not make a profit, as the market price of CH₄ was too low and the electrovalency was too high. However, this does not mean that this technology is not desirable, because it is very promising to use methane as an energy-storage medium for when controlled nuclear fusion is improved or almost all electricity is generated from renewable energy and used as next-generation rocket fuel; the in situ production of methane as rocket fuel on alien planets, such as Mars, will become a key technology in human interstellar navigation. Another interesting point is that the FE of CH₄ has a minor impact on profitability, as its byproduct, hydrogen, is even more expensive.

Table 4. Cash-flow sheet.

Initial Capital Cost (C ₀)		Cash Flow (per Year)	
CO ₂ capture facility	–USD 27 million	Electricity	–USD 64.5 million
Electrolyzer cost	–USD 20 million	Maintenance	–USD 1.49 million
PSA facility	–USD 12.7 million	Cell compartment replacement (normalized to each year)	–USD 1.28 million
		CO ₂ capture	–USD 4 million
		sales of CH ₄	+USD 10.908 million
		sales of H ₂	+USD 10.3 million
total	–USD 59.7 million	total	–USD 50.06 million

6. Conclusions and Outlook

Electrochemical CO₂ reduction has gained considerable attention as an effective means of mitigating environmental pressure due to its eco-friendliness, operational simplicity, and economic efficiency. Of particular interest is the potential for enhancing the selectivity of CH₄ production in the catalytic process. In this review, we presented an overview of the related research on the catalytic mechanisms and catalyst design strategies, providing an assessment of the state-of-the-art work and techno-economic analysis and life cycle assessment of electrochemical CO₂ reduction to methane system, and offering recommendations for future studies.

We briefly described the electrolyte effect to provide a preliminary understanding of the system reactions. With the ongoing research and development, a more thorough understanding of the reaction mechanisms is expected to yield additional strategies for designing high-performance CO₂RR catalysts. A comprehensive mechanistic study, particularly in the reaction pathway catalyzing the multi-electron transfer of CO₂RR for CH₄ formation, is essential to improve catalyst selectivity for CH₄ products.

Moreover, the development of new powerful toolkits, including machine learning, macrodynamic simulations, and operating conditions/in situ techniques, holds promise for advancing our mechanistic understanding. These tools have the potential to yield insights into the underlying processes that govern catalyst performance, facilitating the development of more efficient and effective catalysts for electrochemical CO₂ reductions. Overall, a continued effort in this area of research is essential to address environmental challenges and create a sustainable future. The design and development of catalysts are expected to make significant progress in the future. In this regard, we should make the following efforts in the future:

(1) Improve in situ techniques and apparatus with higher temporal and spatial resolutions to capture key species not previously found experimentally to better understand the reaction mechanism [157,158]. For example, Lu et al. [159] made a breakthrough in the study of the mechanism of the electrocatalytic reduction of CO₂/CO by using advanced techniques, such as electrochemical reaction activity testing and high-pressure in situ spectroscopy. By introducing the strategy of probe molecules acting on the target reaction network, they proposed a new perspective on the surface-coverage level of important intermediates and the CO₂/CO-reduction reaction network, which makes up for the cognitive deficiencies, at present, and provides a new idea for development in this field;

(2) Develop high-throughput syntheses and testing techniques for the rapid and reproducible screening of catalysts. High-throughput approaches are particularly suitable for problems where the parameter space is too large to be effectively solved using conventional methods [160–162]. Catalyst synthesis and testing fit this perfectly, and unsurprisingly, it can help the development of CO₂RR electrocatalysts;

(3) Develop accelerated DFT methods and microscopic dynamics for machine learning modeling. This can help us thoroughly and accurately explain the mechanisms and rapidly predict catalyst materials [163]. Singh et al. [164] developed high-accuracy neural network (NN) ML models for predicting the adsorption energies of COOH*, CO*, and CHO* [165–168]. This work accelerated the development of catalysts and provided an effective strategy to circumvent the scaling relation.

Finally, although the low market price of methane makes it impossible to commercialize electrocatalytic CO₂RR for CH₄ formation, we should consider improving the performance of catalytic materials, such as electrolysis voltage, current density, energy efficiency, and stability, as it is very promising to use methane as an energy-storage medium for when controlled nuclear fusion is improved or almost all electricity is generated from renewable energy and used as next-generation rocket fuel, where the in situ production of methane as rocket fuel on alien planets, such as Mars, will become a key technology in human interstellar navigation. In order to promote the industrialization of electrocatalytic carbon dioxide, we should pay more attention to studies on upstream and downstream processing, process design and techno-economic feasibility.

Author Contributions: Conceptualization, Y.W. and H.D.; validation, P.L., X.Z. and Y.Y.; formal analysis, H.D.; investigation, P.L.; resources, X.Z.; data curation, Y.Y.; writing—original draft preparation, Y.W.; writing—review and editing, Y.W.; visualization, Y.W.; supervision, W.Z.; project administration, W.Z.; funding acquisition, W.Z. All authors have read and agreed to the published version of the manuscript.

Funding: W.Z. would like to acknowledge the support from the National Natural Science Foundation of China (22176086), the Natural Science Foundation of Jiangsu Province (BK20210189), the State Key Laboratory of Pollution Control and Resource Reuse (PCRR-ZZ-202106), the Fundamental Research Funds for the Central Universities (021114380183, 021114380189, 021114380199), the Research Funds from Frontiers Science Center for Critical Earth Material Cycling of Nanjing University, and the Research Funds for Jiangsu Distinguished Professor.

Institutional Review Board Statement: Not applicable.

Informed Consent Statement: Not applicable.

Data Availability Statement: The data presented in this study are openly available in [10.1021/acs.iecr.7b03514], reference number [142].

Conflicts of Interest: The authors declare no conflict of interest.

References

1. Pearson, P.N.; Palmer, M.R. Atmospheric carbon dioxide concentrations over the past 60 million years. *Nature* **2000**, *406*, 695–699. [[CrossRef](#)] [[PubMed](#)]
2. Liu, L.-X.; Fu, J.; Jiang, L.-P.; Zhang, J.-R.; Zhu, W.; Lin, Y. Highly Efficient Photoelectrochemical Reduction of CO₂ at Low Applied Voltage Using 3D Co-Pi/BiVO₄/SnO₂ Nanosheet Array Photoanodes. *ACS Appl. Mater. Interfaces* **2019**, *11*, 26024–26031. [[CrossRef](#)]
3. Brady, J.M. Global Climate Change and Human Health. *J. PeriAnesthesia Nurs.* **2020**, *35*, 89–90. [[CrossRef](#)]
4. Saleemdeeb, R.; Saint, R.; Clark, W.; Lenaghan, M.; Pratt, K.; Millar, F. A pragmatic and industry-oriented framework for data quality assessment of environmental footprint tools. *Resour. Environ. Sustain.* **2021**, *3*, 100019. [[CrossRef](#)]
5. Zhang, D.; Yang, W.; Wang, Z.; Ren, C.; Wang, Y.; Ding, M.; Liu, T. Efficient electrochemical CO₂ reduction reaction on a robust perovskite type cathode with in-situ exsolved Fe-Ru alloy nanocatalysts. *Sep. Purif. Technol.* **2023**, *304*, 122287. [[CrossRef](#)]
6. Yuan, Y.; Lu, J. Demanding energy from carbon. *Carbon Energy* **2019**, *1*, 8–12. [[CrossRef](#)]
7. Wang, G.; Li, X.; Yang, X.; Liu, L.-X.; Cai, Y.; Wu, Y.; Wang, S.; Li, H.; Zhou, Y.; Wang, Y.; et al. Metal-Based Aerogels Catalysts for Electrocatalytic CO₂ Reduction. *Chem.-A Eur. J.* **2022**, *28*, e202201834. [[CrossRef](#)]
8. De Luna, P.; Hahn, C.; Higgins, D.; Jaffer, S.A.; Jaramillo, T.F.; Sargent, E.H. What would it take for renewably powered electrosynthesis to displace petrochemical processes? *Science* **2019**, *364*, aav3506, Erratum in *Science* **2020**, *367*, eabb0992. [[CrossRef](#)] [[PubMed](#)]
9. Liu, Z.; Deng, Z.; He, G.; Wang, H.; Zhang, X.; Lin, J.; Qi, Y.; Liang, X. Challenges and opportunities for carbon neutrality in China. *Nat. Rev. Earth Environ.* **2022**, *3*, 141–155. [[CrossRef](#)]
10. Shi, X.; Zheng, Y.; Lei, Y.; Xue, W.; Yan, G.; Liu, X.; Cai, B.; Tong, D.; Wang, J. Air quality benefits of achieving carbon neutrality in China. *Sci. Total Environ.* **2021**, *795*, 148784. [[CrossRef](#)]
11. Salvia, M.; Reckien, D.; Pietrapertosa, F.; Eckersley, P.; Spyridaki, N.-A.; Krook-Riekkola, A.; Olazabal, M.; De Gregorio Hurtado, S.; Simoes, S.G.; Geneletti, D.; et al. Will climate mitigation ambitions lead to carbon neutrality? An analysis of the local-level plans of 327 cities in the EU. *Renew. Sustain. Energy Rev.* **2021**, *135*, 110253. [[CrossRef](#)]
12. He, M.; Sun, Y.; Han, B. Green Carbon Science: Efficient Carbon Resource Processing, Utilization, and Recycling towards Carbon Neutrality. *Angew. Chem. Int. Ed.* **2022**, *61*, e202112835. [[CrossRef](#)]
13. Liu, Z.; Sun, T.; Yu, Y.; Ke, P.; Deng, Z.; Lu, C.; Huo, D.; Ding, X. Near-Real-Time Carbon Emission Accounting Technology Toward Carbon Neutrality. *Engineering* **2022**, *14*, 44–51. [[CrossRef](#)]
14. Wang, Y.; Godin, R.; Durrant, J.R.; Tang, J. Efficient Hole Trapping in Carbon Dot/Oxygen-Modified Carbon Nitride Heterojunction Photocatalysts for Enhanced Methanol Production from CO₂ under Neutral Conditions. *Angew. Chem. Int. Ed.* **2021**, *60*, 20811–20816. [[CrossRef](#)] [[PubMed](#)]
15. Ajmal, S.; Yasin, G.; Kumar, A.; Tabish, M.; Ibraheem, S.; Sammed, K.A.; Mushtaq, M.A.; Saad, A.; Mo, Z.; Zhao, W. A disquisition on CO₂ electroreduction to C₂H₄: An engineering and design perspective looking beyond novel choosy catalyst materials. *Coord. Chem. Rev.* **2023**, *485*, 215099. [[CrossRef](#)]
16. Wei, J.; Yao, R.; Han, Y.; Ge, Q.; Sun, J. Towards the development of the emerging process of CO₂ heterogenous hydrogenation into high-value unsaturated heavy hydrocarbons. *Chem. Soc. Rev.* **2021**, *50*, 10764–10805. [[CrossRef](#)]
17. Lee, W.J.; Li, C.; Prajitno, H.; Yoo, J.; Patel, J.; Yang, Y.; Lim, S. Recent trend in thermal catalytic low temperature CO₂ methanation: A critical review. *Catal. Today* **2021**, *368*, 2–19. [[CrossRef](#)]

18. Navarro-Jaén, S.; Virginie, M.; Bonin, J.; Robert, M.; Wojcieszak, R.; Khodakov, A.Y. Highlights and challenges in the selective reduction of carbon dioxide to methanol. *Nat. Rev. Chem.* **2021**, *5*, 564–579. [[CrossRef](#)]
19. Shi, D.; Feng, Y.; Zhong, S. Photocatalytic conversion of CH₄ and CO₂ to oxygenated compounds over Cu/CdS–TiO₂/SiO₂ catalyst. *Catal. Today* **2004**, *98*, 505–509. [[CrossRef](#)]
20. Pachaiappan, R.; Rajendran, S.; Senthil Kumar, P.; Vo, D.-V.N.; Hoang, T.K.A. A review of recent progress on photocatalytic carbon dioxide reduction into sustainable energy products using carbon nitride. *Chem. Eng. Res. Des.* **2022**, *177*, 304–320. [[CrossRef](#)]
21. Becker, J.M.; Lielpetere, A.; Szczesny, J.; Junqueira, J.R.C.; Rodríguez-Maciá, P.; Birrell, J.A.; Conzuelo, F.; Schuhmann, W. Bioelectrocatalytic CO₂ Reduction by Redox Polymer-Wired Carbon Monoxide Dehydrogenase Gas Diffusion Electrodes. *ACS Appl. Mater. Interfaces* **2022**, *14*, 46421–46426. [[CrossRef](#)] [[PubMed](#)]
22. Yu, Y.; Chen, L.; Wang, J.; Zhao, Y.; Song, J. Implications of power industry marketization for sustainable generation portfolios in China. *J. Clean. Prod.* **2022**, *378*, 134541. [[CrossRef](#)]
23. Liu, J.; Cai, Y.; Song, R.; Ding, S.; Lyu, Z.; Chang, Y.-C.; Tian, H.; Zhang, X.; Du, D.; Zhu, W.; et al. Recent progress on single-atom catalysts for CO₂ electroreduction. *Mater. Today* **2021**, *48*, 95–114. [[CrossRef](#)]
24. Liu, J.; Fu, J.; Zhou, Y.; Zhu, W.; Jiang, L.-P.; Lin, Y. Controlled Synthesis of EDTA-Modified Porous Hollow Copper Microspheres for High-Efficiency Conversion of CO₂ to Multicarbon Products. *Nano Lett.* **2020**, *20*, 4823–4828. [[CrossRef](#)]
25. Jia, Y.; Li, F.; Fan, K.; Sun, L. Cu-based bimetallic electrocatalysts for CO₂ reduction. *Adv. Powder Mater.* **2022**, *1*, 100012. [[CrossRef](#)]
26. Yin, C.; Li, Q.; Zheng, J.; Ni, Y.; Wu, H.; Kjøniksen, A.-L.; Liu, C.; Lei, Y.; Zhang, Y. Progress in regulating electronic structure strategies on Cu-based bimetallic catalysts for CO₂ reduction reaction. *Adv. Powder Mater.* **2022**, *1*, 100055. [[CrossRef](#)]
27. Gang, Y.; Li, B.; Fang, S.; Pellessier, J.; Fang, L.; Pan, F.; Du, Z.; Hang Hu, Y.; Li, T.; Wang, G.; et al. Efficient electrochemical CO₂ reduction to CO by metal and nitrogen co-doped carbon catalysts derived from pharmaceutical wastes adsorbed on commercial carbon nanotubes. *Chem. Eng. J.* **2023**, *453*, 139712. [[CrossRef](#)]
28. He, Z.; Goulas, J.; Parker, E.; Sun, Y.; Zhou, X.-D.; Fei, L. Review on covalent organic frameworks and derivatives for electrochemical and photocatalytic CO₂ reduction. *Catal. Today* **2023**, *409*, 103–118. [[CrossRef](#)]
29. Lu, X.; Liu, Z.; Zhang, J.-R.; Zhou, Y.; Wang, L.; Zhu, J.-J. General Synergistic Hybrid Catalyst Synthesis Method Using a Natural Enzyme Scaffold-Confined Metal Nanocluster. *ACS Appl. Mater. Interfaces* **2023**, *15*, 761–771. [[CrossRef](#)]
30. Zhao, R.; Ding, P.; Wei, P.; Zhang, L.; Liu, Q.; Luo, Y.; Li, T.; Lu, S.; Shi, X.; Gao, S.; et al. Recent Progress in Electrocatalytic Methanation of CO₂ at Ambient Conditions. *Adv. Funct. Mater.* **2021**, *31*, 2009449. [[CrossRef](#)]
31. Sun, L.; Wang, Y.; Guan, N.; Li, L. Methane Activation and Utilization: Current Status and Future Challenges. *Energy Technol.* **2020**, *8*, 1900826. [[CrossRef](#)]
32. Lunsford, J.H. Catalytic conversion of methane to more useful chemicals and fuels: A challenge for the 21st century. *Catal. Today* **2000**, *63*, 165–174. [[CrossRef](#)]
33. De Souza, R.F.B.; Florio, D.Z.; Antolini, E.; Neto, A.O. Partial Methane Oxidation in Fuel Cell-Type Reactors for Co-Generation of Energy and Chemicals: A Short Review. *Catalysts* **2022**, *12*, 217. [[CrossRef](#)]
34. Divins, N.J.; Braga, A.; Vendrell, X.; Serrano, I.; Garcia, X.; Soler, L.; Lucentini, I.; Danielis, M.; Mussio, A.; Colussi, S.; et al. Investigation of the evolution of Pd-Pt supported on ceria for dry and wet methane oxidation. *Nat. Commun.* **2022**, *13*, 5080. [[CrossRef](#)]
35. Song, H.; Ye, J. Direct photocatalytic conversion of methane to value-added chemicals. *Trends Chem.* **2022**, *4*, 1094–1105. [[CrossRef](#)]
36. Kang, Y.; Tian, M.; Huang, C.; Lin, J.; Hou, B.; Pan, X.; Li, L.; Rykov, A.I.; Wang, J.; Wang, X. Improving Syngas Selectivity of Fe₂O₃/Al₂O₃ with Yttrium Modification in Chemical Looping Methane Conversion. *ACS Catal.* **2019**, *9*, 8373–8382. [[CrossRef](#)]
37. Karakaya, C.; Kee, R.J. Progress in the direct catalytic conversion of methane to fuels and chemicals. *Prog. Energy Combust. Sci.* **2016**, *55*, 60–97. [[CrossRef](#)]
38. Sun, Z.; Russell, C.K.; Whitty, K.J.; Eddings, E.G.; Dai, J.; Zhang, Y.; Fan, M.; Sun, Z. Chemical looping-based energy transformation via lattice oxygen modulated selective oxidation. *Prog. Energy Combust. Sci.* **2023**, *96*, 101045. [[CrossRef](#)]
39. Arutyunov, V.; Savchenko, V.; Sedov, I.; Arutyunov, A.; Nikitin, A. The Fuel of Our Future: Hydrogen or Methane? *Methane* **2022**, *1*, 96–106. [[CrossRef](#)]
40. Freund, H.J.; Roberts, M.W. Surface chemistry of carbon dioxide. *Surf. Sci. Rep.* **1996**, *25*, 225–273. [[CrossRef](#)]
41. Marković, N.M.; Ross, P.N. Surface science studies of model fuel cell electrocatalysts. *Surf. Sci. Rep.* **2002**, *45*, 117–229. [[CrossRef](#)]
42. Aui, A.; Wang, Y.; Mba-Wright, M. Evaluating the economic feasibility of cellulosic ethanol: A meta-analysis of techno-economic analysis studies. *Renew. Sustain. Energy Rev.* **2021**, *145*, 111098. [[CrossRef](#)]
43. Wang, X.; Li, P.; Cao, Y.; Hong, W.; Geng, Z.; An, Z.; Wang, H.; Wang, H.; Sun, B.; Zhu, W.; et al. Techno-economic Analysis and Industrial Application Prospects of Single-atom Materials in CO₂ Catalysis. *Chem. J. Chin. Univ.* **2022**, *43*, 20220347.
44. Woodson, M.S.; Jablonowski, C.J. An Economic Assessment of Traditional and Cellulosic Ethanol Technologies. *Energy Sources Part B* **2008**, *3*, 372–383. [[CrossRef](#)]
45. Yousaf, M.; Mahmood, A.; Elkamel, A.; Rizwan, M.; Zaman, M. Techno-economic analysis of integrated hydrogen and methanol production process by CO₂ hydrogenation. *Int. J. Greenh. Gas Control* **2022**, *115*, 103615. [[CrossRef](#)]
46. Hara, K.; Kudo, A.; Sakata, T. Electrochemical CO₂ reduction on a glassy carbon electrode under high pressure. *J. Electroanal. Chem.* **1997**, *421*, 1–4. [[CrossRef](#)]
47. Schouten, K.J.P.; Kwon, Y.; van der Ham, C.J.M.; Qin, Z.; Koper, M.T.M. A new mechanism for the selectivity to C1 and C2 species in the electrochemical reduction of carbon dioxide on copper electrodes. *Chem. Sci.* **2011**, *2*, 1902–1909. [[CrossRef](#)]

48. Yu, P.; Lv, X.; Wang, Q.; Huang, H.; Weng, W.; Peng, C.; Zhang, L.; Zheng, G. Promoting Electrocatalytic CO₂ Reduction to CH₄ by Copper Porphyrin with Donor–Acceptor Structures. *Small* **2023**, *19*, 2205730. [[CrossRef](#)]
49. Xuan, X.; Cheng, J.; Yang, X.; Zhou, J. Highly Selective Electrochemical Reduction of CO₂ to CH₄ over Vacancy–Metal–Nitrogen Sites in an Artificial Photosynthetic Cell. *ACS Sustain. Chem. Eng.* **2020**, *8*, 1679–1686. [[CrossRef](#)]
50. Hatsukade, T.; Kuhl, K.P.; Cave, E.R.; Abram, D.N.; Jaramillo, T.F. Insights into the electrocatalytic reduction of CO₂ on metallic silver surfaces. *Phys. Chem. Chem. Phys.* **2014**, *16*, 13814–13819. [[CrossRef](#)]
51. Nie, X.; Luo, W.; Janik, M.J.; Asthagiri, A. Reaction mechanisms of CO₂ electrochemical reduction on Cu(111) determined with density functional theory. *J. Catal.* **2014**, *312*, 108–122. [[CrossRef](#)]
52. Dong, H.; Li, Y.; Jiang, D.-E. First-Principles Insight into Electrocatalytic Reduction of CO₂ to CH₄ on a Copper Nanoparticle. *J. Phys. Chem. C* **2018**, *122*, 11392–11398. [[CrossRef](#)]
53. Chan, K. A few basic concepts in electrochemical carbon dioxide reduction. *Nat. Commun.* **2020**, *11*, 5954. [[CrossRef](#)]
54. Ge, L.; Rabiee, H.; Li, M.; Subramanian, S.; Zheng, Y.; Lee, J.H.; Burdyny, T.; Wang, H. Electrochemical CO₂ reduction in membrane-electrode assemblies. *Chem* **2022**, *8*, 663–692. [[CrossRef](#)]
55. Kortlever, R.; Shen, J.; Schouten, K.J.P.; Calle-Vallejo, F.; Koper, M.T.M. Catalysts and Reaction Pathways for the Electrochemical Reduction of Carbon Dioxide. *J. Phys. Chem. Lett.* **2015**, *6*, 4073–4082. [[CrossRef](#)]
56. Peterson, A.A.; Nørskov, J.K. Activity Descriptors for CO₂ Electroreduction to Methane on Transition-Metal Catalysts. *J. Phys. Chem. Lett.* **2012**, *3*, 251–258. [[CrossRef](#)]
57. Jitaru, M.; Lowy, D.A.; Toma, M.; Toma, B.C.; Oniciu, L. Electrochemical reduction of carbon dioxide on flat metallic cathodes. *J. Appl. Electrochem.* **1997**, *27*, 875–889. [[CrossRef](#)]
58. Dutta, A.; Morstein, C.E.; Rahaman, M.; Cedeño López, A.; Broekmann, P. Beyond Copper in CO₂ Electrolysis: Effective Hydrocarbon Production on Silver-Nanofoam Catalysts. *ACS Catal.* **2018**, *8*, 8357–8368. [[CrossRef](#)]
59. Du, H.; Fu, J.; Liu, L.-X.; Ding, S.; Lyu, Z.; Chang, Y.-C.; Jin, X.; Kengara, F.O.; Song, B.; Min, Q.; et al. Recent progress in electrochemical reduction of carbon monoxide toward multi-carbon products. *Mater. Today* **2022**, *59*, 182–199. [[CrossRef](#)]
60. Frese, K.W. Chapter 6—ELECTROCHEMICAL REDUCTION OF CO₂ AT SOLID ELECTRODES. In *Electrochemical and Electrocatalytic Reactions of Carbon Dioxide*; Sullivan, B.P., Ed.; Elsevier: Amsterdam, The Netherlands, 1993; pp. 145–216. [[CrossRef](#)]
61. Deng, B.; Huang, M.; Li, K.; Zhao, X.; Geng, Q.; Chen, S.; Xie, H.; Dong, X.a.; Wang, H.; Dong, F. The Crystal Plane is not the Key Factor for CO₂-to-Methane Electrosynthesis on Reconstructed Cu₂O Microparticles. *Angew. Chem. Int. Ed.* **2022**, *61*, e202114080. [[CrossRef](#)] [[PubMed](#)]
62. Schreier, M.; Yoon, Y.; Jackson, M.N.; Surendranath, Y. Competition between H and CO for Active Sites Governs Copper-Mediated Electrosynthesis of Hydrocarbon Fuels. *Angew. Chem. Int. Ed.* **2018**, *57*, 10221–10225. [[CrossRef](#)]
63. Liang, S.; Altaf, N.; Huang, L.; Gao, Y.; Wang, Q. Electrolytic cell design for electrochemical CO₂ reduction. *J. CO₂ Util.* **2020**, *35*, 90–105. [[CrossRef](#)]
64. Stuve, E.M. Electrochemical Reactor Design and Configurations. In *Encyclopedia of Applied Electrochemistry*; Kreysa, G., Ota, K.-I., Savinell, R.F., Eds.; Springer: New York, NY, USA, 2014; pp. 568–578. [[CrossRef](#)]
65. Noël, T.; Cao, Y.; Laudadio, G. The Fundamentals Behind the Use of Flow Reactors in Electrochemistry. *Acc. Chem. Res.* **2019**, *52*, 2858–2869. [[CrossRef](#)]
66. Gao, D.; Arán-Ais, R.M.; Jeon, H.S.; Roldan Cuenya, B. Rational catalyst and electrolyte design for CO₂ electroreduction towards multicarbon products. *Nat. Catal.* **2019**, *2*, 198–210. [[CrossRef](#)]
67. Urakawa, A. Mind the gaps in CO₂-to-methanol. *Nat. Catal.* **2021**, *4*, 447–448. [[CrossRef](#)]
68. Gupta, N.; Gattrell, M.; MacDougall, B. Calculation for the cathode surface concentrations in the electrochemical reduction of CO₂ in KHCO₃ solutions. *J. Appl. Electrochem.* **2006**, *36*, 161–172. [[CrossRef](#)]
69. Wu, J.; Zheng, W.; Chen, Y. Factors affecting the cathode/electrolyte interfacial pH change during water reduction: A simulation study. *Int. J. Hydrog. Energy* **2022**, *47*, 18597–18605. [[CrossRef](#)]
70. Kühn, S.P.; Edström, K.; Winter, M.; Cekic-Laskovic, I. Face to Face at the Cathode Electrolyte Interphase: From Interface Features to Interphase Formation and Dynamics. *Adv. Mater. Interfaces* **2022**, *9*, 2102078. [[CrossRef](#)]
71. Ma, M.; Deng, W.; Xu, A.; Hochfilzer, D.; Qiao, Y.; Chan, K.; Chorkendorff, I.; Seger, B. Local reaction environment for selective electroreduction of carbon monoxide. *Energy Environ. Sci.* **2022**, *15*, 2470–2478. [[CrossRef](#)]
72. Gattrell, M.; Gupta, N.; Co, A. A review of the aqueous electrochemical reduction of CO₂ to hydrocarbons at copper. *J. Electroanal. Chem.* **2006**, *594*, 1–19. [[CrossRef](#)]
73. Resasco, J.; Chen, L.D.; Clark, E.; Tsai, C.; Hahn, C.; Jaramillo, T.F.; Chan, K.; Bell, A.T. Promoter Effects of Alkali Metal Cations on the Electrochemical Reduction of Carbon Dioxide. *J. Am. Chem. Soc.* **2017**, *139*, 11277–11287. [[CrossRef](#)] [[PubMed](#)]
74. Peng, J.; Cao, D.; He, Z.; Guo, J.; Hapala, P.; Ma, R.; Cheng, B.; Chen, J.; Xie, W.J.; Li, X.-Z.; et al. The effect of hydration number on the interfacial transport of sodium ions. *Nature* **2018**, *557*, 701–705. [[CrossRef](#)] [[PubMed](#)]
75. Gonella, G.; Backus, E.H.G.; Nagata, Y.; Bonthuis, D.J.; Loche, P.; Schlaich, A.; Netz, R.R.; Kühnle, A.; McCrum, I.T.; Koper, M.T.M.; et al. Water at charged interfaces. *Nat. Rev. Chem.* **2021**, *5*, 466–485. [[CrossRef](#)]
76. Rebstock, J.A.; Zhu, Q.; Baker, L.R. Comparing interfacial cation hydration at catalytic active sites and spectator sites on gold electrodes: Understanding structure sensitive CO₂ reduction kinetics. *Chem. Sci.* **2022**, *13*, 7634–7643. [[CrossRef](#)] [[PubMed](#)]
77. Singh, M.R.; Kwon, Y.; Lum, Y.; Ager, J.W., III; Bell, A.T. Hydrolysis of Electrolyte Cations Enhances the Electrochemical Reduction of CO₂ over Ag and Cu. *J. Am. Chem. Soc.* **2016**, *138*, 13006–13012. [[CrossRef](#)]

78. Monteiro, M.C.O.; Dattila, F.; Hagedoorn, B.; García-Muelas, R.; López, N.; Koper, M.T.M. Absence of CO₂ electroreduction on copper, gold and silver electrodes without metal cations in solution. *Nat. Catal.* **2021**, *4*, 654–662. [[CrossRef](#)]
79. Liu, M.; Pang, Y.; Zhang, B.; De Luna, P.; Voznyy, O.; Xu, J.; Zheng, X.; Dinh, C.T.; Fan, F.; Cao, C.; et al. Enhanced electrocatalytic CO₂ reduction via field-induced reagent concentration. *Nature* **2016**, *537*, 382–386. [[CrossRef](#)]
80. Ni, J.; Cheng, Q.; Liu, S.; Wang, M.; He, Y.; Qian, T.; Yan, C.; Lu, J. Deciphering Electrolyte Selection for Electrochemical Reduction of Carbon Dioxide and Nitrogen to High-Value-Added Chemicals. *Adv. Funct. Mater.* **2023**, *33*, 2212483. [[CrossRef](#)]
81. Kaneco, S.; Katsumata, H.; Suzuki, T.; Ohta, K. Electrochemical Reduction of CO₂ to Methane at the Cu Electrode in Methanol with Sodium Supporting Salts and Its Comparison with Other Alkaline Salts. *Energy Fuels* **2006**, *20*, 409–414. [[CrossRef](#)]
82. Moura de Salles Pupo, M.; Kortlever, R. Electrolyte Effects on the Electrochemical Reduction of CO₂. *ChemPhysChem* **2019**, *20*, 2926–2935. [[CrossRef](#)]
83. Deng, B.; Huang, M.; Zhao, X.; Mou, S.; Dong, F. Interfacial Electrolyte Effects on Electrocatalytic CO₂ Reduction. *ACS Catal.* **2022**, *12*, 331–362. [[CrossRef](#)]
84. König, M.; Vaes, J.; Klemm, E.; Pant, D. Solvents and Supporting Electrolytes in the Electrocatalytic Reduction of CO₂. *iScience* **2019**, *19*, 135–160. [[CrossRef](#)] [[PubMed](#)]
85. Hung, S.-F.; Xu, A.; Wang, X.; Li, F.; Hsu, S.-H.; Li, Y.; Wicks, J.; Cervantes, E.G.; Rasouli, A.S.; Li, Y.C.; et al. A metal-supported single-atom catalytic site enables carbon dioxide hydrogenation. *Nat. Commun.* **2022**, *13*, 819. [[CrossRef](#)]
86. Cai, Y.; Fu, J.; Zhou, Y.; Chang, Y.-C.; Min, Q.; Zhu, J.-J.; Lin, Y.; Zhu, W. Insights on forming N,O-coordinated Cu single-atom catalysts for electrochemical reduction CO₂ to methane. *Nat. Commun.* **2021**, *12*, 586. [[CrossRef](#)]
87. Chang, C.-J.; Lin, S.-C.; Chen, H.-C.; Wang, J.; Zheng, K.J.; Zhu, Y.; Chen, H.M. Dynamic Reoxidation/Reduction-Driven Atomic Interdiffusion for Highly Selective CO₂ Reduction toward Methane. *J. Am. Chem. Soc.* **2020**, *142*, 12119–12132. [[CrossRef](#)]
88. Wang, Y.; Chen, J.; Wang, G.; Li, Y.; Wen, Z. Perfluorinated Covalent Triazine Framework Derived Hybrids for the Highly Selective Electroconversion of Carbon Dioxide into Methane. *Angew. Chem. Int. Ed.* **2018**, *57*, 13120–13124. [[CrossRef](#)]
89. Yang, Y.-L.; Wang, Y.-R.; Dong, L.-Z.; Li, Q.; Zhang, L.; Zhou, J.; Sun, S.-N.; Ding, H.-M.; Chen, Y.; Li, S.-L.; et al. A Honeycomb-Like Porous Crystalline Hetero-Electrocatalyst for Efficient Electrocatalytic CO₂ Reduction. *Adv. Mater.* **2022**, *34*, 2206706. [[CrossRef](#)] [[PubMed](#)]
90. Han, L.; Song, S.; Liu, M.; Yao, S.; Liang, Z.; Cheng, H.; Ren, Z.; Liu, W.; Lin, R.; Qi, G.; et al. Stable and Efficient Single-Atom Zn Catalyst for CO₂ Reduction to CH₄. *J. Am. Chem. Soc.* **2020**, *142*, 12563–12567. [[CrossRef](#)] [[PubMed](#)]
91. Manthiram, K.; Beberwyck, B.J.; Alivisatos, A.P. Enhanced Electrochemical Methanation of Carbon Dioxide with a Dispersible Nanoscale Copper Catalyst. *J. Am. Chem. Soc.* **2014**, *136*, 13319–13325. [[CrossRef](#)]
92. Li, Y.; Cui, F.; Ross, M.B.; Kim, D.; Sun, Y.; Yang, P. Structure-Sensitive CO₂ Electroreduction to Hydrocarbons on Ultrathin 5-fold Twinned Copper Nanowires. *Nano Lett.* **2017**, *17*, 1312–1317. [[CrossRef](#)]
93. Wang, Z.; Yuan, Q.; Shan, J.; Jiang, Z.; Xu, P.; Hu, Y.; Zhou, J.; Wu, L.; Niu, Z.; Sun, J.; et al. Highly Selective Electrocatalytic Reduction of CO₂ into Methane on Cu–Bi Nanoalloys. *J. Phys. Chem. Lett.* **2020**, *11*, 7261–7266. [[CrossRef](#)] [[PubMed](#)]
94. Zhang, L.; Li, X.-X.; Lang, Z.-L.; Liu, Y.; Liu, J.; Yuan, L.; Lu, W.-Y.; Xia, Y.-S.; Dong, L.-Z.; Yuan, D.-Q.; et al. Enhanced Cuprophilic Interactions in Crystalline Catalysts Facilitate the Highly Selective Electroreduction of CO₂ to CH₄. *J. Am. Chem. Soc.* **2021**, *143*, 3808–3816. [[CrossRef](#)] [[PubMed](#)]
95. Zhou, X.; Shan, J.; Chen, L.; Xia, B.Y.; Ling, T.; Duan, J.; Jiao, Y.; Zheng, Y.; Qiao, S.-Z. Stabilizing Cu²⁺ Ions by Solid Solutions to Promote CO₂ Electroreduction to Methane. *J. Am. Chem. Soc.* **2022**, *144*, 2079–2084. [[CrossRef](#)]
96. Lin, L.; Liu, T.; Xiao, J.; Li, H.; Wei, P.; Gao, D.; Nan, B.; Si, R.; Wang, G.; Bao, X. Enhancing CO₂ Electroreduction to Methane with a Cobalt Phthalocyanine and Zinc–Nitrogen–Carbon Tandem Catalyst. *Angew. Chem. Int. Ed.* **2020**, *59*, 22408–22413. [[CrossRef](#)] [[PubMed](#)]
97. Xiong, L.; Zhang, X.; Chen, L.; Deng, Z.; Han, S.; Chen, Y.; Zhong, J.; Sun, H.; Lian, Y.; Yang, B.; et al. Geometric Modulation of Local CO Flux in Ag@Cu₂O Nanoreactors for Steering the CO₂RR Pathway toward High-Efficacy Methane Production. *Adv. Mater.* **2021**, *33*, 2101741. [[CrossRef](#)]
98. Wang, G.; Chen, J.; Ding, Y.; Cai, P.; Yi, L.; Li, Y.; Tu, C.; Hou, Y.; Wen, Z.; Dai, L. Electrocatalysis for CO₂ conversion: From fundamentals to value-added products. *Chem. Soc. Rev.* **2021**, *50*, 4993–5061. [[CrossRef](#)]
99. Lu, B.; Liu, Q.; Chen, S. Electrocatalysis of Single-Atom Sites: Impacts of Atomic Coordination. *ACS Catal.* **2020**, *10*, 7584–7618. [[CrossRef](#)]
100. Etim, U.J.; Zhang, C.; Zhong, Z. Impacts of the Catalyst Structures on CO₂ Activation on Catalyst Surfaces. *Nanomaterials* **2021**, *11*, 3265. [[CrossRef](#)]
101. Li, H.; Qin, X.; Jiang, T.; Ma, X.-Y.; Jiang, K.; Cai, W.-B. Changing the Product Selectivity for Electrocatalysis of CO₂ Reduction Reaction on Plated Cu Electrodes. *ChemCatChem* **2019**, *11*, 6139–6146. [[CrossRef](#)]
102. Bernal Lopez, M.; Ustarroz, J. Electrodeposition of nanostructured catalysts for electrochemical energy conversion: Current trends and innovative strategies. *Curr. Opin. Electrochem.* **2021**, *27*, 100688. [[CrossRef](#)]
103. Connor, P.; Schuch, J.; Kaiser, B.; Jaegermann, W. The Determination of Electrochemical Active Surface Area and Specific Capacity Revisited for the System MnOx as an Oxygen Evolution Catalyst. *Z. Für Phys. Chem.* **2020**, *234*, 979–994. [[CrossRef](#)]
104. Mistry, H.; Varela, A.S.; Kühn, S.; Strasser, P.; Cuenya, B.R. Nanostructured electrocatalysts with tunable activity and selectivity. *Nat. Rev. Mater.* **2016**, *1*, 16009. [[CrossRef](#)]

105. Zhu, W.; Zhang, Y.-J.; Zhang, H.; Lv, H.; Li, Q.; Michalsky, R.; Peterson, A.A.; Sun, S. Active and Selective Conversion of CO₂ to CO on Ultrathin Au Nanowires. *J. Am. Chem. Soc.* **2014**, *136*, 16132–16135. [[CrossRef](#)] [[PubMed](#)]
106. Cometto, C.; Ugolotti, A.; Graziotti, E.; Moretto, A.; Bottaro, G.; Armelao, L.; Di Valentin, C.; Calvillo, L.; Granozzi, G. Copper single-atoms embedded in 2D graphitic carbon nitride for the CO₂ reduction. *NPJ 2D Mater. Appl.* **2021**, *5*, 63. [[CrossRef](#)]
107. Wheeler, D.A.; Wang, G.; Ling, Y.; Li, Y.; Zhang, J.Z. Nanostructured hematite: Synthesis, characterization, charge carrier dynamics, and photoelectrochemical properties. *Energy Environ. Sci.* **2012**, *5*, 6682–6702. [[CrossRef](#)]
108. Reske, R.; Mistry, H.; Behafarid, F.; Roldan Cuenya, B.; Strasser, P. Particle Size Effects in the Catalytic Electroreduction of CO₂ on Cu Nanoparticles. *J. Am. Chem. Soc.* **2014**, *136*, 6978–6986. [[CrossRef](#)] [[PubMed](#)]
109. Loiodice, A.; Lobaccaro, P.; Kamali, E.A.; Thao, T.; Huang, B.H.; Ager, J.W.; Buonsanti, R. Tailoring Copper Nanocrystals towards C₂ Products in Electrochemical CO₂ Reduction. *Angew. Chem. Int. Ed.* **2016**, *55*, 5789–5792. [[CrossRef](#)]
110. Yao, J.; Yao, Y. Zeolite supported Pd electrocatalyst nanoparticle characterization. *Int. J. Hydrog. Energy* **2019**, *44*, 287–294. [[CrossRef](#)]
111. Miola, M.; Hu, X.-M.; Brandiele, R.; Bjerglund, E.T.; Grønseth, D.K.; Durante, C.; Pedersen, S.U.; Lock, N.; Skrydstrup, T.; Daasbjerg, K. Ligand-free gold nanoparticles supported on mesoporous carbon as electrocatalysts for CO₂ reduction. *J. CO₂ Util.* **2018**, *28*, 50–58. [[CrossRef](#)]
112. Lim, D.-H.; Jo, J.H.; Shin, D.Y.; Wilcox, J.; Ham, H.C.; Nam, S.W. Carbon dioxide conversion into hydrocarbon fuels on defective graphene-supported Cu nanoparticles from first principles. *Nanoscale* **2014**, *6*, 5087–5092. [[CrossRef](#)]
113. Chen, H.; Liang, X.; Liu, Y.; Ai, X.; Asefa, T.; Zou, X. Active Site Engineering in Porous Electrocatalysts. *Adv. Mater.* **2020**, *32*, 2002435. [[CrossRef](#)] [[PubMed](#)]
114. Su, Z.; Chen, T. Porous Noble Metal Electrocatalysts: Synthesis, Performance, and Development. *Small* **2021**, *17*, 2005354. [[CrossRef](#)]
115. Zhang, Y.; Lan, P.C.; Martin, K.; Ma, S. Porous frustrated Lewis pair catalysts: Advances and perspective. *Chem Catal.* **2022**, *2*, 439–457. [[CrossRef](#)]
116. Zhao, L.; Lan, Z.; Mo, W.; Su, J.; Liang, H.; Yao, J.; Yang, W. High-Level Oxygen Reduction Catalysts Derived from the Compounds of High-Specific-Surface-Area Pine Peel Activated Carbon and Phthalocyanine Cobalt. *Nanomater* **2021**, *11*, 3429. [[CrossRef](#)] [[PubMed](#)]
117. Lv, J.-J.; Jouny, M.; Luc, W.; Zhu, W.; Zhu, J.-J.; Jiao, F. A Highly Porous Copper Electrocatalyst for Carbon Dioxide Reduction. *Adv. Mater.* **2018**, *30*, 1803111. [[CrossRef](#)] [[PubMed](#)]
118. Furukawa, H.; Cordova, K.E.; O’Keeffe, M.; Yaghi, O.M. The Chemistry and Applications of Metal-Organic Frameworks. *Science* **2013**, *341*, 1230444. [[CrossRef](#)]
119. Zhang, Y.; Dong, L.-Z.; Li, S.; Huang, X.; Chang, J.-N.; Wang, J.-H.; Zhou, J.; Li, S.-L.; Lan, Y.-Q. Coordination environment dependent selectivity of single-site-Cu enriched crystalline porous catalysts in CO₂ reduction to CH₄. *Nat. Commun.* **2021**, *12*, 6390. [[CrossRef](#)]
120. Xu, H.; Cheng, D.; Cao, D.; Zeng, X.C. A universal principle for a rational design of single-atom electrocatalysts. *Nat. Catal.* **2018**, *1*, 339–348. [[CrossRef](#)]
121. Chen, Y.; Ji, S.; Chen, C.; Peng, Q.; Wang, D.; Li, Y. Single-Atom Catalysts: Synthetic Strategies and Electrochemical Applications. *Joule* **2018**, *2*, 1242–1264. [[CrossRef](#)]
122. Mu, Y.; Wang, T.; Zhang, J.; Meng, C.; Zhang, Y.; Kou, Z. Single-Atom Catalysts: Advances and Challenges in Metal-Support Interactions for Enhanced Electrocatalysis. *Electrochem. Energy Rev.* **2022**, *5*, 145–186. [[CrossRef](#)]
123. Shin, S.; Haaring, R.; So, J.; Choi, Y.; Lee, H. Highly Durable Heterogeneous Atomic Catalysts. *Acc. Chem. Res.* **2022**, *55*, 1372–1382. [[CrossRef](#)]
124. Zitolo, A.; Goellner, V.; Armel, V.; Sougrati, M.-T.; Mineva, T.; Stievano, L.; Fonda, E.; Jaouen, F. Identification of catalytic sites for oxygen reduction in iron- and nitrogen-doped graphene materials. *Nat. Mater.* **2015**, *14*, 937–942. [[CrossRef](#)]
125. Yang, X.-F.; Wang, A.; Qiao, B.; Li, J.; Liu, J.; Zhang, T. Single-Atom Catalysts: A New Frontier in Heterogeneous Catalysis. *Acc. Chem. Res.* **2013**, *46*, 1740–1748. [[CrossRef](#)]
126. Wang, Y.; Chen, Z.; Han, P.; Du, Y.; Gu, Z.; Xu, X.; Zheng, G. Single-Atomic Cu with Multiple Oxygen Vacancies on Ceria for Electrocatalytic CO₂ Reduction to CH₄. *ACS Catal.* **2018**, *8*, 7113–7119. [[CrossRef](#)]
127. Kuhl, K.P.; Cave, E.R.; Abram, D.N.; Jaramillo, T.F. New insights into the electrochemical reduction of carbon dioxide on metallic copper surfaces. *Energy Environ. Sci.* **2012**, *5*, 7050–7059. [[CrossRef](#)]
128. Abild-Pedersen, F.; Greeley, J.; Studt, F.; Rossmeisl, J.; Munter, T.R.; Moses, P.G.; Skúlason, E.; Bligaard, T.; Nørskov, J.K. Scaling Properties of Adsorption Energies for Hydrogen-Containing Molecules on Transition-Metal Surfaces. *Phys. Rev. Lett.* **2007**, *99*, 016105. [[CrossRef](#)]
129. Kuhl, K.P.; Hatsukade, T.; Cave, E.R.; Abram, D.N.; Kibsgaard, J.; Jaramillo, T.F. Electrocatalytic Conversion of Carbon Dioxide to Methane and Methanol on Transition Metal Surfaces. *J. Am. Chem. Soc.* **2014**, *136*, 14107–14113. [[CrossRef](#)] [[PubMed](#)]
130. Li, Q.; Fu, J.; Zhu, W.; Chen, Z.; Shen, B.; Wu, L.; Xi, Z.; Wang, T.; Lu, G.; Zhu, J.-J.; et al. Tuning Sn-Catalysis for Electrochemical Reduction of CO₂ to CO via the Core/Shell Cu/SnO₂ Structure. *J. Am. Chem. Soc.* **2017**, *139*, 4290–4293. [[CrossRef](#)] [[PubMed](#)]
131. Zeng, S.; Shan, S.; Lu, A.; Wang, S.; Caracciolo, D.T.; Robinson, R.J.; Shang, G.; Xue, L.; Zhao, Y.; Zhang, A.; et al. Copper-alloy catalysts: Structural characterization and catalytic synergies. *Catal. Sci. Technol.* **2021**, *11*, 5712–5733. [[CrossRef](#)]

132. Kim, D.; Resasco, J.; Yu, Y.; Asiri, A.M.; Yang, P. Synergistic geometric and electronic effects for electrochemical reduction of carbon dioxide using gold–copper bimetallic nanoparticles. *Nat. Commun.* **2014**, *5*, 4948. [[CrossRef](#)]
133. Xiao, Z.; Wu, H.; Zhong, H.; Abdelhafiz, A.; Zeng, J. De-alloyed PtCu/C catalysts with enhanced electrocatalytic performance for the oxygen reduction reaction. *Nanoscale* **2021**, *13*, 13896–13904. [[CrossRef](#)]
134. Liu, D.; Huang, H.-Z.; Zhu, Z.; Li, J.; Chen, L.-W.; Jing, X.-T.; Yin, A.-X. Promoting the Electrocatalytic Ethanol Oxidation Activity of Pt by Alloying with Cu. *Catalysts* **2022**, *12*, 1562. [[CrossRef](#)]
135. Ponc, V. Alloy catalysts: The concepts. *Appl. Catal. A Gen.* **2001**, *222*, 31–45. [[CrossRef](#)]
136. Zhu, W.; Tackett, B.M.; Chen, J.G.; Jiao, F. Bimetallic Electrocatalysts for CO₂ Reduction. *Top. Curr. Chem.* **2018**, *376*, 41. [[CrossRef](#)]
137. Dong, W.J.; Yoo, C.J.; Lim, J.W.; Park, J.Y.; Kim, K.; Kim, S.; Lee, D.; Lee, J.-L. Tailoring electronic structure of bifunctional Cu/Ag layered electrocatalysts for selective CO₂ reduction to CO and CH₄. *Nano Energy* **2020**, *78*, 105168. [[CrossRef](#)]
138. Zhou, Y.; Che, F.; Liu, M.; Zou, C.; Liang, Z.; De Luna, P.; Yuan, H.; Li, J.; Wang, Z.; Xie, H.; et al. Dopant-induced electron localization drives CO₂ reduction to C₂ hydrocarbons. *Nat. Chem.* **2018**, *10*, 974–980. [[CrossRef](#)] [[PubMed](#)]
139. Tan, X.; Yu, C.; Zhao, C.; Huang, H.; Yao, X.; Han, X.; Guo, W.; Cui, S.; Huang, H.; Qiu, J. Restructuring of Cu₂O to Cu₂O@Cu-Metal–Organic Frameworks for Selective Electrochemical Reduction of CO₂. *ACS Appl. Mater. Interfaces* **2019**, *11*, 9904–9910. [[CrossRef](#)]
140. Mistry, H.; Reske, R.; Zeng, Z.; Zhao, Z.-J.; Greeley, J.; Strasser, P.; Cuenya, B.R. Exceptional Size-Dependent Activity Enhancement in the Electroreduction of CO₂ over Au Nanoparticles. *J. Am. Chem. Soc.* **2014**, *136*, 16473–16476. [[CrossRef](#)] [[PubMed](#)]
141. Kim, C.; Jeon, H.S.; Eom, T.; Jee, M.S.; Kim, H.; Friend, C.M.; Min, B.K.; Hwang, Y.J. Achieving Selective and Efficient Electrocatalytic Activity for CO₂ Reduction Using Immobilized Silver Nanoparticles. *J. Am. Chem. Soc.* **2015**, *137*, 13844–13850. [[CrossRef](#)] [[PubMed](#)]
142. Jouny, M.; Luc, W.; Jiao, F. General Techno-Economic Analysis of CO₂ Electrolysis Systems. *Ind. Eng. Chem. Res.* **2018**, *57*, 2165–2177. [[CrossRef](#)]
143. Gao, W.; Liang, S.; Wang, R.; Jiang, Q.; Zhang, Y.; Zheng, Q.; Xie, B.; Toe, C.Y.; Zhu, X.; Wang, J.; et al. Industrial carbon dioxide capture and utilization: State of the art and future challenges. *Chem. Soc. Rev.* **2020**, *49*, 8584–8686. [[CrossRef](#)] [[PubMed](#)]
144. Patnaik, D.; Pattanaik, A.K.; Bagal, D.K.; Rath, A. Reducing CO₂ emissions in the iron industry with green hydrogen. *Int. J. Hydrog. Energy* **2023**, in press. [[CrossRef](#)]
145. Ozkan, M.; Akhavi, A.-A.; Coley, W.C.; Shang, R.; Ma, Y. Progress in carbon dioxide capture materials for deep decarbonization. *Chem* **2022**, *8*, 141–173. [[CrossRef](#)]
146. Tong, Y.; Wang, K.; Liu, J.; Zhang, Y.; Gao, J.; Dan, M.; Yue, T.; Zuo, P.; Zhao, Z. Refined assessment and decomposition analysis of carbon emissions in high-energy intensive industrial sectors in China. *Sci. Total Environ.* **2023**, *872*, 162161. [[CrossRef](#)]
147. Wei, K.; Guan, H.; Luo, Q.; He, J.; Sun, S. Recent advances in CO₂ capture and reduction. *Nanoscale* **2022**, *14*, 11869–11891. [[CrossRef](#)] [[PubMed](#)]
148. Sabatino, F.; Grimm, A.; Gallucci, F.; van Sint Annaland, M.; Kramer, G.J.; Gazzani, M. A comparative energy and costs assessment and optimization for direct air capture technologies. *Joule* **2021**, *5*, 2047–2076. [[CrossRef](#)]
149. Sullivan, I.; Goryachev, A.; Digdaya, I.A.; Li, X.; Atwater, H.A.; Vermaas, D.A.; Xiang, C. Coupling electrochemical CO₂ conversion with CO₂ capture. *Nat. Catal.* **2021**, *4*, 952–958. [[CrossRef](#)]
150. Kukobat, R.; Sakai, M.; Tanaka, H.; Otsuka, H.; Vallejos-Burgos, F.; Lastoskie, C.; Matsukata, M.; Sasaki, Y.; Yoshida, K.; Hayashi, T.; et al. Ultrapermeable 2D-channelled graphene-wrapped zeolite molecular sieving membranes for hydrogen separation. *Sci. Adv.* **2022**, *8*, eabl3521. [[CrossRef](#)]
151. Du, P.; Zhang, Y.; Wang, X.; Canossa, S.; Hong, Z.; Nénert, G.; Jin, W.; Gu, X. Control of zeolite framework flexibility for ultra-selective carbon dioxide separation. *Nat. Commun.* **2022**, *13*, 1427. [[CrossRef](#)] [[PubMed](#)]
152. Abd, A.A.; Othman, M.R.; Helwani, Z.; Kim, J. Waste to wheels: Performance comparison between pressure swing adsorption and amine-absorption technologies for upgrading biogas containing hydrogen sulfide to fuel grade standards. *Energy* **2023**, *272*, 127060. [[CrossRef](#)]
153. Shin, H.; Hansen, K.U.; Jiao, F. Techno-economic assessment of low-temperature carbon dioxide electrolysis. *Nat. Sustain.* **2021**, *4*, 911–919. [[CrossRef](#)]
154. Ramdin, M.; De Mot, B.; Morrison, A.R.T.; Breugelmanns, T.; van den Broeke, L.J.P.; Trusler, J.P.M.; Kortlever, R.; de Jong, W.; Moulto, O.A.; Xiao, P.; et al. Electroreduction of CO₂/CO to C₂ Products: Process Modeling, Downstream Separation, System Integration, and Economic Analysis. *Ind. Eng. Chem. Res.* **2021**, *60*, 17862–17880. [[CrossRef](#)] [[PubMed](#)]
155. Luberti, M.; Ahn, H. Review of Polybed pressure swing adsorption for hydrogen purification. *Int. J. Hydrog. Energy* **2022**, *47*, 10911–10933. [[CrossRef](#)]
156. Augelletti, R.; Frattari, S.; Murmura, M.A. Purification of Hydrogen-Methane Mixtures Using PSA Technology. In *Enriched Methane: The First Step towards the Hydrogen Economy*; De Falco, M., Basile, A., Eds.; Springer International Publishing: Cham, Switzerland, 2016; pp. 129–146. [[CrossRef](#)]
157. Buckley, S.; Brackin, R.; Näsholm, T.; Schmidt, S.; Jämtgård, S. Improving in situ recovery of soil nitrogen using the microdialysis technique. *Soil Biol. Biochem.* **2017**, *114*, 93–103. [[CrossRef](#)]
158. Wang, Y.; Huang, C.; Hu, J.; Wang, M. Development of high-resolution spatio-temporal models for ambient air pollution in a metropolitan area of China from 2013 to 2019. *Chemosphere* **2022**, *291*, 132918. [[CrossRef](#)]

159. Malkani, A.S.; Li, J.; Oliveira, N.J.; He, M.; Chang, X.; Xu, B.; Lu, Q. Understanding the electric and nonelectric field components of the cation effect on the electrochemical CO reduction reaction. *Sci. Adv.* **2020**, *6*, eabd2569. [[CrossRef](#)]
160. Murphy, V.; Volpe, A.F.; Weinberg, W.H. High-throughput approaches to catalyst discovery. *Curr. Opin. Chem. Biol.* **2003**, *7*, 427–433. [[CrossRef](#)]
161. Tandoc, C.; Hu, Y.-J.; Qi, L.; Liaw, P.K. Mining of lattice distortion, strength, and intrinsic ductility of refractory high entropy alloys. *NPJ Comput. Mater.* **2023**, *9*, 53. [[CrossRef](#)]
162. Baudis, S.; Behl, M. High-Throughput and Combinatorial Approaches for the Development of Multifunctional Polymers. *Macromol. Rapid Commun.* **2022**, *43*, 2100400. [[CrossRef](#)]
163. Pederson, R.; Kalita, B.; Burke, K. Machine learning and density functional theory. *Nat. Rev. Phys.* **2022**, *4*, 357–358. [[CrossRef](#)]
164. Chen, Z.W.; Garipey, Z.; Chen, L.; Yao, X.; Anand, A.; Liu, S.-J.; Tetsassi Feugmo, C.G.; Tamblyn, I.; Singh, C.V. Machine-Learning-Driven High-Entropy Alloy Catalyst Discovery to Circumvent the Scaling Relation for CO₂ Reduction Reaction. *ACS Catal.* **2022**, *12*, 14864–14871. [[CrossRef](#)]
165. Farris, B.R.; Niang-Trost, T.; Branicky, M.S.; Leonard, K.C. Evaluation of Machine Learning Models on Electrochemical CO₂ Reduction Using Human Curated Datasets. *ACS Sustain. Chem. Eng.* **2022**, *10*, 10934–10944. [[CrossRef](#)]
166. Hu, E.; Liu, C.; Zhang, W.; Yan, Q. Machine Learning Assisted Understanding and Discovery of CO₂ Reduction Reaction Electrocatalyst. *J. Phys. Chem. C* **2023**, *127*, 882–893. [[CrossRef](#)]
167. Zhong, M.; Tran, K.; Min, Y.; Wang, C.; Wang, Z.; Dinh, C.-T.; De Luna, P.; Yu, Z.; Rasouli, A.S.; Brodersen, P.; et al. Accelerated discovery of CO₂ electrocatalysts using active machine learning. *Nature* **2020**, *581*, 178–183. [[CrossRef](#)] [[PubMed](#)]
168. Xing, M.; Zhang, Y.; Li, S.; He, H.; Sun, S. Prediction of Carbon Dioxide Reduction Catalyst Using Machine Learning with a Few-Feature Model: WLEDZ. *J. Phys. Chem. C* **2022**, *126*, 17025–17035. [[CrossRef](#)]

Disclaimer/Publisher's Note: The statements, opinions and data contained in all publications are solely those of the individual author(s) and contributor(s) and not of MDPI and/or the editor(s). MDPI and/or the editor(s) disclaim responsibility for any injury to people or property resulting from any ideas, methods, instructions or products referred to in the content.